Track MS status:
May 4th 2025 – First version submitted to EarthArXiv and Earth Science Reviews (Elsevier)
May 7th 2025 – Editorial rejection (out of scope for a large review journal)
May 9th, 2025 – Submitted to *Quaternary Science Reviews* (Elsevier)
September 12th, 2025 – Rejected after reviews, possible resubmission indicated by editor
December 27th, 2025 – Revised MS produced, submitted to *Geomorphology* (Elsevier)

The Apalachicola Barrier Island complex: a benchmark for MIS 5e (125 ka) sea-level oscillations?

Nikos Georgiou[1], Alexander R. Simms[2], Roger C. Creel[3], Silas Dean[1], Denovan Chauveau[4], Ciro Cerrone[1], Claudia Caporizzo[5], Alessio Rovere[1,6]

[1] University of Venice Ca' Foscari, Department of Environmental Sciences, Informatics and Statistics, Scientific Campus Via Torino 155, 30172 Mestre (VE), Italy
[2] Department of Earth Science, University of California Santa Barbara, Santa Barbara, CA 93106, USA
[3] Woods Hole Oceanographic Institution, Woods Hole, Massachusetts 02543-1050, USA
[4] Geo-Ocean, UMR 6538, CNRS, Ifremer, Université de Bretagne Occidentale, F-29280 Plouzané, France
[5] Università Telematica Pegaso, Centro Direzionale Isola F2, 80143, Napoli, Italy
[6] MARUM, Center for Marine Environmental Sciences, University of Bremen, Leobener Str. 8, 28359 Bremen, Germany

Correspondence to: Alessio Rovere (alessio.rovere@unive.it)

Abstract

The geomorphological and stratigraphic framework of coastal sandy barrier systems preserve records of past sea-level changes, climatic shifts, and storm histories. Recent methodological advances such as Ground Penetrating Radar (GPR), LiDAR topography, and Optically Stimulated Luminescence (OSL) dating now allow for high-resolution reconstructions of these past coastal dynamics, significantly improving our understanding of historical shoreline evolution. Using new GPR and existing LIDAR and OSL ages, we investigate the evolution of the Apalachicola Barrier Island Complex in northwest Florida during the Pleistocene including the Last Interglacial (MIS 5e, ~125 ka). Paleogeographic reconstructions show significant barrier morphological changes, including island segmentation and deltaic interactions over multiple highstands including not only MIS5e but potentially older highstands (e.g. MIS7 or older). We find evidence within the Apalachicola complex for two distinct phases of beach ridge growth potentially linked to early and late MIS 5e sea-level highstands, separated by an erosional unconformity marking a mid-MIS 5e regression and fluvial incision, potentially marking an oscillation in MIS5e sea levels. GPR profiles also record multiple buried storm scarps, indicating major storms approximately every 76years, assuming similar progradation rates during MIS5e as during the Holocene. Furthermore, the potential oscillation in RSL at this site in the Gulf of Mexico adds to recent suggestions of a regrowth of the Antarctic Ice Sheet following its collapse during late MIS5e.

1. Introduction

Sedimentary coastal systems respond to different forcings by prograding (i.e., advancing horizontally), retreating and accreting (growing vertically) as a response to changes in sea level (Okazaki et al., 2022), storm intensity and direction (Buynevich et al., 2007; Goodwin et al., 2023; Lindhorst and Schutter, 2014), sediment supply, and shoreline evolution (Dougherty, 2018). Prograding sand barriers serve as near-continuous records of paleoenvironmental signals, and studies on their evolution have advanced in the last decades thanks to the development of techniques such as Light Detection and Ranging (LiDAR), Ground Penetrating Radar (GPR), and Optically Stimulated Luminescence (OSL) dating (Fairbridge and Hillaire-Marcel, 1977; Gernant et al., 2025; Rodriguez and Meyer, 2006; Scheffers et al., 2012). These methods allow high-resolution studies of surface and subsurface morphological features and provide chronological constraints on the evolution of sandy barriers.

Prograded sandy coastal barriers are depositional landforms found globally in a range of geological, climatic, and sea-level contexts (Otvos, 2000). They can develop during both rising and falling sea levels (Boyd et al., 1992). Typically, they form in shallow and flat coastal areas with sufficient accommodation and substantial sediment supplies, sourced from either fluvial or long/cross-shore transport (Scheffers et al., 2012). Moderate wave energy is also an important factor in their formation and maintenance. Wave energy needs to be strong enough to move sediment above the mean spring tide level, but not so strong that erosion exceeds deposition. Beyond sediment discharge, wind, storms, and tidal range also govern the beach ridge morphology of prograding sandy coastal barriers (Isla et al., 2023; Tamura, 2012). When sediment accumulation exceeds available accommodation, coastal barriers advance seaward, forming beach ridges systems that preserve near-continuous paleoclimatic and morphodynamic geo-archives (Hein and Ashton, 2020). Under regressive conditions, these systems manifest as sequences of beach ridges and spits, while barrier islands and estuarine strandplains form under transgressive conditions (Isla et al., 2023).

While studies on Holocene beach ridges are widespread within prograding sandy barriers, fewer studies have examined Pleistocene beach ridges, which are generally found landward of their Holocene counterparts. In this paper, we use GPR data from beach ridges along the Apalachicola composite barrier system in Florida (US Gulf Coast) along with high-resolution DEMs and a reanalysis of existing OSL ages to shed light on sea-level oscillations and storm frequency along the Apalachicola beach barrier complex during the Pleistocene including the Last Interglacial (Marine Isotopic Stage, MIS , 5e, 125 ka).

2. Background

2.1 *Beach Ridges as archives of past environmental changes*

On the horizontal plane (Supplementary Figure 1), beach ridge systems are represented by shore-parallel to semi-parallel prograding series of ridges and swales (Taylor and Stone, 1996). Their pronounced relief is usually attributed to the development of a foredune ridge due to the aeolian sand trapped by vegetation on the back barrier. However, lower relief

ridges might form without the presence of an aeolian cap, with the berm's role in shaping this relief though still under debate (Hesp, 1984). In the vertical plane (Supplementary Figure 2), internal architecture of beach ridges can be revealed using GPR surveys. Prograding paleo-beachfaces are expressed as seaward-inclined deposits with their inclination varying up to 6° (fine-coarse sand) (Tamura, 2012), being steeper for coarser grains (Jol et al., 1996) and lower wave energy (Hede et al., 2013; Phillips et al., 2019).

Beach ridges are regularly used to reconstruct past sea levels (Gernant et al., 2025; Kumar et al., 2024; Mauz et al., 2013; Montes et al., 2018; Stattegger et al., 2013). Specific elements within beach ridge systems have been used as Sea Level Index Points (SLIPs), that indicate past sea-level positions in space and time (Shennan, 1986; Shennan et al., 2015). Within beach ridges the facies most commonly used as SLIPs include the Beach-Dune contact, the berm, the Beachface-Upper shoreface contact, and the Upper-Lower shoreface contact (Costas et al., 2016; Tamura et al., 2007). The Beach-Dune (hereafter BD) contact is the uppermost SLIP in a beach ridge and marks the maximum runup of storm waves. On GPR sonograms, this is identifies as a series of strong, wavy, sub-horizontal, subparallel reflections, with the dipping beachface below showing truncation or toplap structures (Costas et al., 2016). The wave berm, characterized by a flat or landward sloping platform and a slope change at its seaward margin, marks the upper limit of the fairweather swash zone (Costas et al., 2016; Otvos, 2000). Seaward-dipping reflections of the beachface downlap onto the upper shoreface indicate average low-tide sea levels and are also considered reliable SLIPs as they capture both high and low sea levels and are the last to erode from the foreshore facies (Hede et al., 2013; Nielsen et al., 2017). The erosional contact between the upper and lower shoreface, created by longshore trough migration, can also be a SLIP, though its precision depends on local wave-breaking depth (Hede et al., 2013).

Variations in sediment flux, whether of anthropogenic or climatic origin, directly affect the beach ridge frequency and spacing over timescales ranging from months to millennia (Hein and Ashton, 2020; Tamura, 2012). Sediment-starved areas tend to form foredune ridges of higher relief and wider spacing compared to the sediment-rich areas marked by quickly prograding beaches (Carvalho et al., 2019; Nooren et al., 2017; Ruz and Allard, 1994), since sediment starvation leaves dunes more time to accumulate aeolian sand prior to being blocked by a newer dune created during beach progradation. The inverse pattern applies for quickly prograding beach units: higher spatial frequency and lower temporal frequency occurring under conditions of high sediment flux.

Minor variations in wave energy, not including destructive or extreme events, can significantly alter the geometry of the beach face as it alternates between dissipative phases that represent high wave energy events and reflective phases deposited under normal wave conditions (Flemming, 1982; Masselink et al., 2006). Storms cause rapid changes along sandy coasts, affecting prograding beach and dune systems, which preserve geological records of these events, both as depositional and erosional landforms (Goslin and Clemmensen, 2017). Storms can form build-ups (i.e. high beach ridges), which usually consist of coarse-grained material (coarse sand, shells, gravel) and may be the result of single or multiple storm events (Carter, 1986;

Butler, 1999). Washover deposits, which contain heavy-minerals, organic content, and shell concentrations, can provide evidence of past storm occurrence and intensity (Goslin and Clemmensen, 2017). They can be recognised by the high energy, landward dipping or horizontal reflectors on GPR profiles of back-barrier sediments, which may form perched fans, sheetwashes, or large scale inlet channels, depending on storm intensity (Carruthers et al., 2013; Donnelly et al., 2006; Masselink and van Heteren, 2014). Even if unconsolidated, large foredunes in prograding beaches prevent storms from breaching barriers, forming erosional scarps by eroding sediments and building bars offshore, which are integrated when the beach is restored back to the reflective profile (Buynevich et al., 2007). These erosional storm scarps are preserved in prograding coasts due to the post-storm recovery infill and, when dated, can record paleo-storm frequency and intensity (Zurbuchen et al., 2020). They are recorded in GPR profiles as high reflectivity, steep seaward dipping strata, and in sediment cores are characterized by heavy minerals (percentage >50%) and coarse-grained material (Dougherty, 2018; Komar and Wang, 1984).

2.2 The Apalachicola Barrier Island Complex

The "Apalachicola Barrier Island Complex" (Rink and López, 2010) consists of Pleistocene beach ridge deposits landward of a Holocene transgressive barrier chain extending from St Joseph Peninsula to the west to St George barrier island to the east (Burdette et al., 2012, Figure 1). It is one of the most extensive strandplains in the Gulf of Mexico, with an ~10 km-wide area of discontinuous Pleistocene beach ridges and 6 km of Holocene beach ridges. Sediment is supplied to the strandplain from the Apalachicola River. The Holocene strandplain is shaped by the prevailing Southern swells. A northwards prograding spit (St. Joseph Peninsula) and three strandplains prograding towards the south (Cape San Blas, St. Vincent Isl., Little St. George Isl.) constitute the main Holocene coastal barrier system, with the narrow SW-NE extending wave-dominated barrier island of St. George bounding the transgressive Apalachicola Bay to the East (Figure 1B).

The Apalachicola Barrier Island Complex is the youngest of a series of off-lapping Plio-Pleistocene sandy, presumably marine, sedimentary formations. The northmost separately mapped unit is the Citronelle Formation (*Tci* in Figure 1A), which consists mainly of quartz sand and gravel, partly deposited as river delta deposits of a late Pliocene-Early Pleistocene nearshore environment (Scott et al., 2001). Seaward of the Citronelle Formation, the Quaternary coastal surface sediments in and around the Apalachicola Delta include Quaternary Holocene sediments (Qh), Quaternary Beach Ridge and Dune (Qbd), Quaternary Alluvium (Qal), and Tertiary/Quaternary Shelly Sediments (TQSu). Otvos (1992) called the second and fourth of these units the Gulfport and Biloxi Formations, respectively, but they were not formally adopted by Scott et al. (2001) in the most recent Florida Geological Survey map. The Quaternary Holocene Sediments (*Qh*) are mainly marine sands, muds and organic matter (peat) near the present coastline. The Quaternary Beach Ridge and Dune (*Qbd*) sediments are composed of beach ridge belts usually consisting of shoreface to foreshore sand. The Quaternary Alluvium (*Qal*) is Pleistocene and Holocene in age and occurs mainly in floodplains. The Tertiary/Quaternary Shelly Sediments (*TQSu*) include mainly nearshore fine-grained fossiliferous sediment.

The age of the Quaternary Beach Ridge and Dune (*Qbd*) is controversial: Burdette et al., (2012) use OSL ages retrieved from coastal sediment cores to suggest that the beach ridges formed during the MIS5e highstand. However, deeper sediment cores from the area suggest that the *Qbd* deposits thicken west of the Apalachicola delta, and are composed of two fining upwards sandy Pleistocene sequences, the younger one dated to ~30 ka and the older attributed to MIS5e (Schnable and Goodell, 1968). *Qal* was interpreted as an alluvial cover of MIS6 age overlying the *TQSu*, but Otvos (1992) highlighted inconsistencies in dating and stratigraphic identification of the *Qal* unit. The formation below the *Qbd* and *Qal* (namely, *TQSu*), showed an OSL saturated signal (Burdette et al., 2012) suggesting an older age (MIS7/9) than the MIS 5 age proposed by Otvos, (1992). To the east of these units, extensive erosion reveals the underlying Miocene-Pliocene formations (Figure 1A).

Immediately inland of the Holocene coastal barriers, a series of older Pleistocene strandplains are present in the Apalachicola area. The ones closest to the Holocene sequence were attributed to the Last Interglacial (MIS 5e, 125 ka, Burdette et al., 2012); the existence of deposits dating to previous Interglacials (MIS7,9) or to the MIS6 lowstand in the broader Apalachicola area (*Qu* formation in Figure 1A) was excluded by Otvos (1992) but supported by Donoghue et al., (1998). The only work providing radiometric ages for Pleistocene coastal sequences in this area is Burdette et al., (2012), who detected a MIS6 alluvium deposit and a fossiliferous nearshore fine-grained formation older than MIS6 (OSL saturated signal) and designated as *TQsu* on geological maps (Scott et al., 2001) and as the Biloxi formation by Otvos, 1992, shown as underlying the MIS6 alluvial deposit and the MIS5e beach ridges.

The marine origin of the older and higher Pleistocene terraces and their interpretation as arcuate sand bodies and barrier islands on the unconsolidated and undifferentiated sediments (*Qu* – sand, clay, organics) of the Apalachicola Delta has been contested. Otvos (1995) suggest that these features may be formed by regional tectonic uplift, human activity, e.g. abandoned logging railroad beds and routes or dissolution of underlying carbonates. Conversely, Donoghue et al. (1998) argue for a marine origin of these formations based on sedimentological and geomorphological data (Brenneman and Tanner, 1958; Goetschius, 1971; Stapor Jr et al., 1991), the subsidence of the area (Holdahl and Morrison, 1974). Ionium-disequilibrium dates indicate ages older than MIS5e for these formations (Maxwell, 1971a, 1971b).

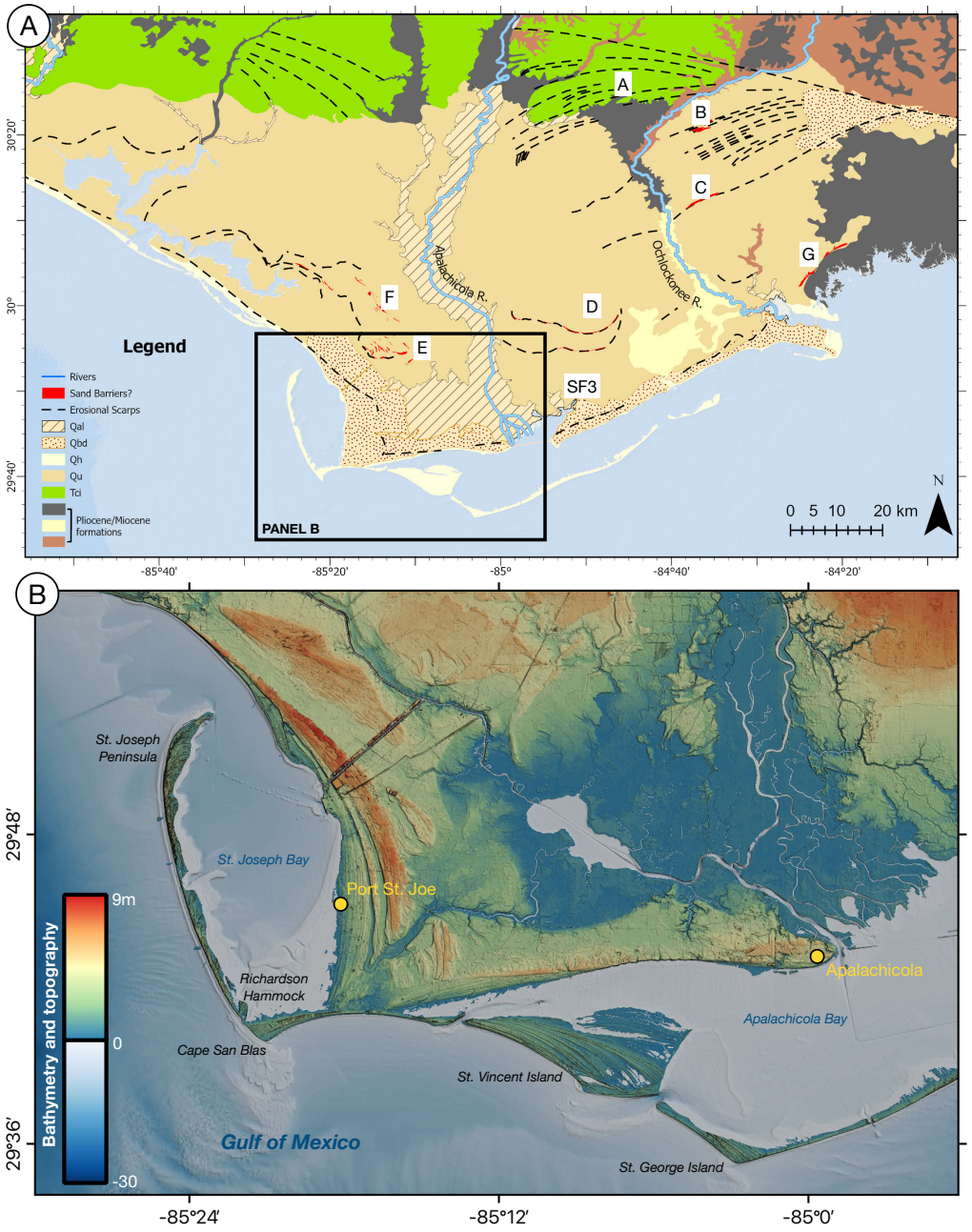

Figure 1. A) Geologic map of the Apalachicola barrier system (from Scott et al., 2001). Red polygons mark sand barriers; dashed black line marks distinct geomorphological features based on the results of former studies. Labels a-g correspond to locations of geomorphological features shown in Figure 2. Label SF3 marks the location of the geomorphological feature represented in Supplementary Figure 3. Legend of geological formations: Qh = Quaternary Holocene Sediments; Qbd = Quaternary Beach Ridge and Dune; Qal = Quaternary Alluvium; Qu = unconsolidated and undifferentiated sediments; Tci = Citronelle Formation. B). Digital elevation model of the study area (NOAA National Centers for Environmental Information, 2023; US Geological Survey, 2011) with toponyms mentioned in the text and main towns.

3. Methods

To better understand the evolution of the Apalachicola delta, we use the 1/9 arcsecond (~3m) and 1-meter Digital Elevation Models (DEM) from Apalachicola to Pensacola (Figure 1B, US Geological Survey, 2022, 2011) and a detailed geological map (Scott et al., 2001) to interpret the geomorphology of the Apalachicola Delta Area. We focused on linear structures marking potential former shorelines (dashed black lines in Figure 1A). In addition to the remote sensing mapping, we visited the more seaward linear structures in the field.

To characterize the subsurface stratigraphy of the most prominent Pleistocene beach barriers in the Apalachicola area and aid in their geomorphic interpretation, we collected 9 km of GPR data using a Sensors and Software EkkoPulse Pro with a 200 MHz antenna. Common-midpoint (CMP) surveys were conducted at each of our six GPR survey sites to determine the velocity of the radar waves within the subsurface. Velocities from these CMP surveys ranged from 0.043 to 0.082 m/ns. GPR profiles were topographically corrected using Global Navigation Satellite System (GNSS) survey data collected at the same time as the GPR. Processing of the GPR lines included automatic gain control and DeWow (a proprietary Sensors and Software processing algorithm). GPR profiles were loaded into EkkoView Deluxe software and ArcMap for interpretation. We assume that the vertical error associated with the identification of a point in the GPR profile is ±0.8m (1-sigma) based on the variability in radar velocities found throughout the area.

GNSS data were collected with a pair EMLID REACH RS+ receivers (single band) working in Real-Time-Kinematics (RTK) configuration. The position of the base station was initially set to uncorrected coordinates in the field and was corrected in post-processing using the FLCB permanent GNSS station (maintained by the Florida Department of Transportation, located 60-70km from our study area). All elevation data were referenced to NAVD88 from the GNSS ellipsoid height using the online VDATUM tool by the US National Oceanic and Atmospheric Administration (https://vdatum.noaa.gov/vdatumweb/). Overall, we estimate that the vertical accuracy of this type of positioning is ±0.2m (1-sigma), including errors due to base postprocessing, rover-base positioning and vertical datum accuracy.

To reconstruct paleo relative sea level (RSL) from the Beach-Dune (BD) contact identified on GPR profiles, its indicative meaning and associated uncertainty is needed (Shennan, 1986; Shennan et al., 2015). We quantify the BD contact indicative meaning by surveying the modern beach-dune contact in GPR profiles at three locations in the study area (Figure 3). Two are at Salinas Park on the east side of Cape San Blas (Lines 85 and 86, Figure 3A); the third is at a public beach access between Lafayette Drive and Martinique Drive on the west side of Cape San Blas (Line 83, Figure 3A).

4. Results and Interpretations

4.1 DEM Mapping

Selective fluvial erosion in a SW-NE orientation within the Citronelle Formation formed wedge-shaped channels whose geometry resembles the landforms of the progradational Holocene throughout the modern Apalachicola Delta. These SW-NE mounds, possibly related to prograding beach deposits, reach maximum elevations of 40m to 56m (vertical datum: NAVD88, Figure 2A).

South of these higher and presumably older units, the crests of the curvilinear landforms range in elevation from 30 to 38m (NAVD88) and are better preserved and of higher relief (Figure 2B, Figure 1A) than those in the Citronelle Formation. An erosional scarp, oriented SW-NE at the base of this unit occurs at an elevation of 20m (NAVD88, Figure 2C). The same scarp extends to the southwest (Figure 2C) along the front of a landform interpreted by Donoghue et al. (1998) as a sandbar but whose interpretation is questioned by Otvos (1995). Revisiting these interpretations with higher-resolution DEMs based on LIDAR surveys seems to confirm Donoghue's model as very similar, but better preserved, younger features resembling barriers are observed at lower elevations on both sides of the Apalachicola River (Figure 2D, E, F). These include seaward concave features (Figure 2D) resembling delta fronts (Olariu and Bhattacharya, 2006) on the east side of the Apalachicola River with high-relief seaward crests at elevations of 9.5-10m and 7-7.5m and wide flat areas (base - Figure 2D) at 7.5-8m and 6m respectively (NAVD88), seaward of the crests. South of these features, cuspate forelands dipping southwards are apparent (Supplementary Figure 3). On the west side of the river, sandy barrier-like features have crest tops at +6m average elevation, while the surrounding base lies at +5m (NAVD88, Figure 2E). To the NW, these features continue but at increasing elevations, reaching a maximum crest elevations of +9m and base elevations at +7m (NAVD88) (Figure 1A, Figure 2F), with a characteristic spit-end feature (Figure 2F inset) at the northeast end. On the eastern side, both sides of the Ochlockonee River have evidence of erosional scarps and spit-barrier features; the features on the river's east side are more prominent (Figure 2G) and have barrier crests from +8-10.5m and a scarp carved at +5m (NAVD88).

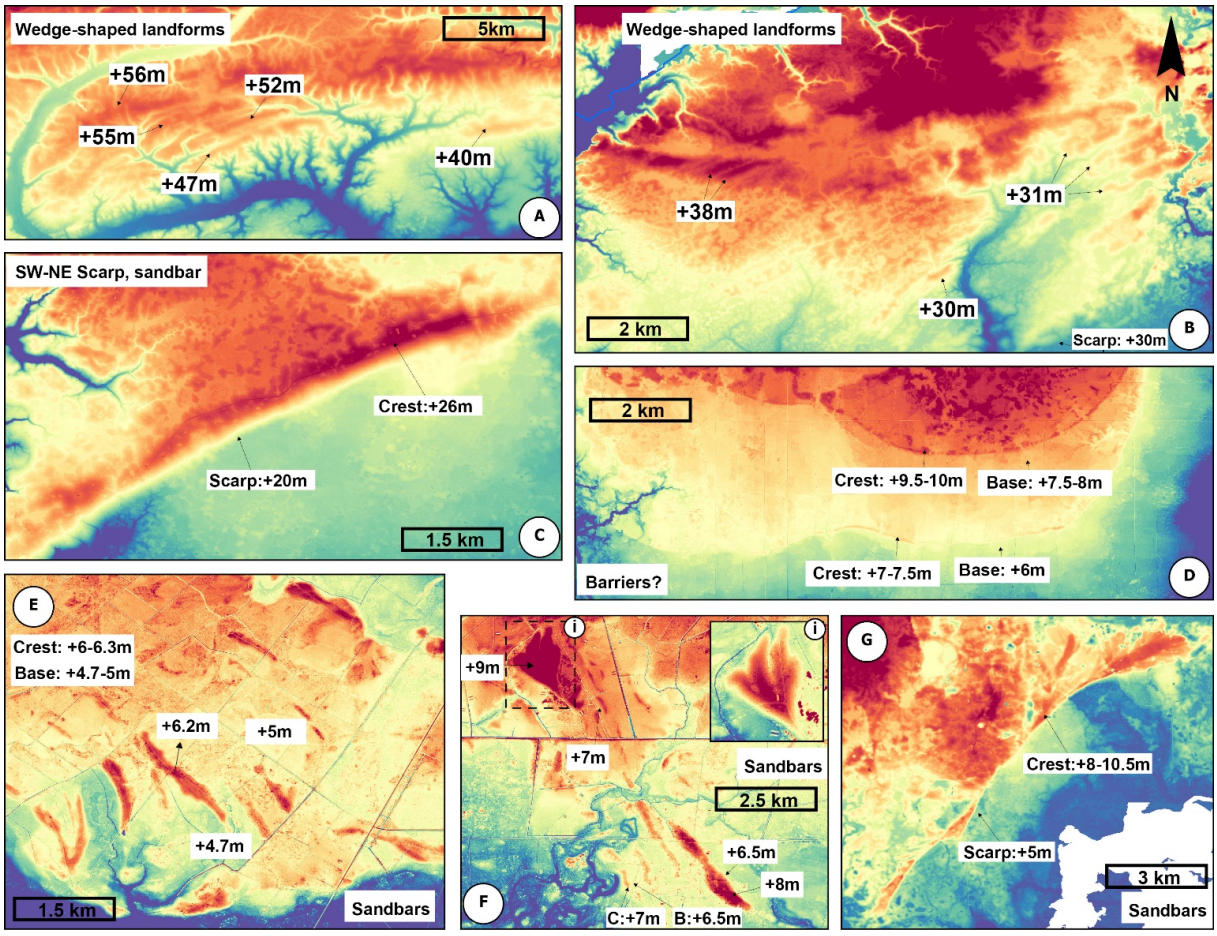

Figure 2. Distinct geomorphological features related to coastal depositional/erosional features. The location of each panel is shown in Figure 1A. Elevation data from 1-meter DEMs (US Geological Survey, 2022).

Seaward of these ridges and south of the Intracoastal Waterway, are no fewer than 3 well-defined ridge sets (Figure 3A). The more landward of these, Beach Ridge Set C, is about 3km wide and reaches a top crest elevation of 9m. Beach Ridge Sets B and A, are lower in elevation ranging from 6-8m and 2-5m, respectively. They are narrower than Beach Ridge Set C, with average widths of 1.5-2 km. Beach Ridge Set A appears to be a younger continuation of Beach Ridge Set B. Beach Ridge Sets B and A are separated by a trough reaching its lower elevation at 1-2m above sea level.

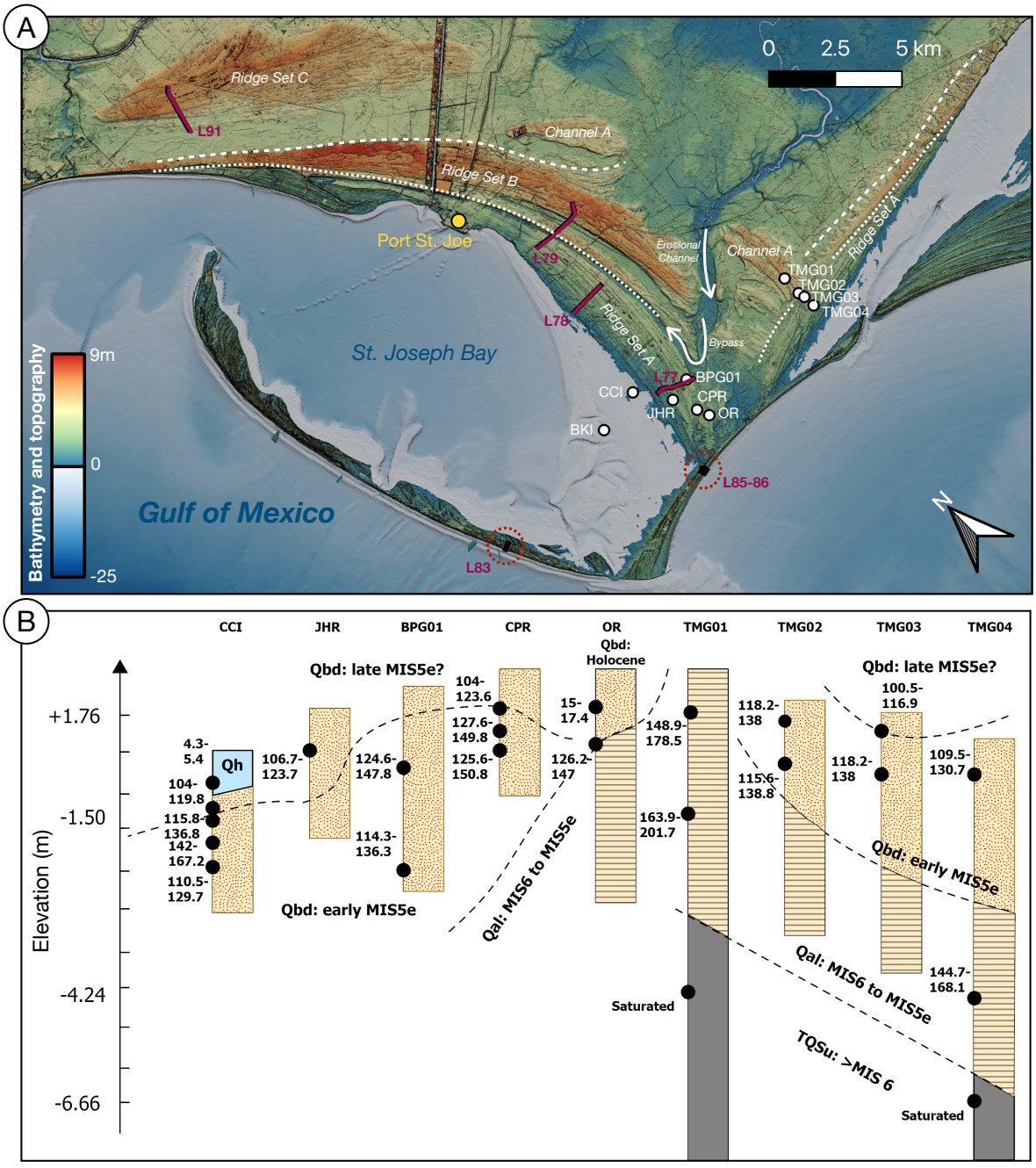

245 **Figure 3**. A) Interpretation of Apalachicola's beach ridge system ages, and correlation with sediment cores from Burdette et al., 2012 (reproduced in Panel B). Elevation data from 1-meter DEMs and bathymetry from NOAA (NOAA National Centers for Environmental Information, 2023; US Geological Survey, 2022).

4.2 Ground Penetrating Radar Stratigraphy and Interpretations

4.2.1 Indicative meaning

Altogether, GPR profiles along the present-day beach (Figure 4A) indicate that the BD contact is, on average, 0.92±0.46m (1-sigma) above modern sea level (Figure 4B). This represents the average and standard deviation of the contact measured in the field, and translates into a reference water level of 0.92m (indicating that the BD contact forms, on average, 0.92m above present-day sea level) and an indicative range (i.e., the elevational range occupied by the Bd contact) of 0.92m (double of the uncertainty range on the BD contact elevation). Therefore, to calculate paleo RSL from the BD contact measured in Pleistocene deposits, 0.92m should be subtracted from the elevation of the BD contact. The final uncertainty of paleo RSL equals the square root of the sum of squares of i) half of the indicative range (0.46m), ii) GPR vertical error (0.8m), and iii) GNSS error (0.2m). By summing this errors using the sum of squares under root mean square formula, the total error associated with paleo RSL is ±0.94m (1-sigma).

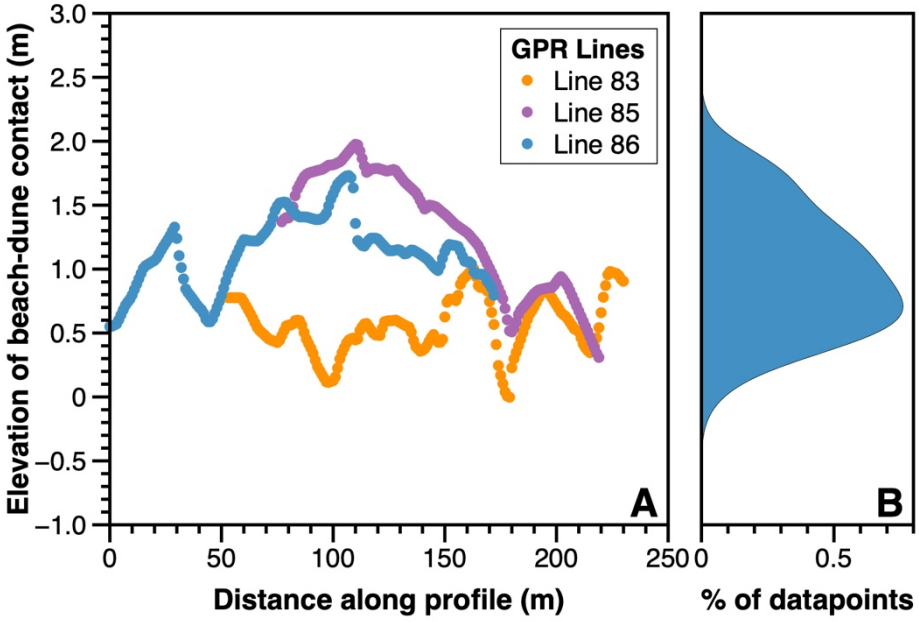

Figure 4 A) Beach-Dune contact identified along GPR lines across the modern shoreline. B) Density plot of the Beach-Dune contact at the three sites. Elevations are referred to the NAVD88 vertical datum.

4.2.1 GPR facies

Three main radar facies were identified in the GPR profiles collected through beach ridge sets A-C and the modern beach. The first radar facies, RF_{sd}, is composed of sets of parallel, seaward dipping reflections. Based on its locations in GPR profiles from the modern beach as well as the generally sandy nature of the deposits underlying this facies, we interpret the RF_{sd} facies to represent foreshore and upper shoreface deposits of a prograding beach/barrier system. The second radar facies, RF_{ld}, is composed of parallel, landward dipping reflections. This radar facies is usually found behind or on the back side of shore-parallel ridges (Line 79, Supplementary Figure 5). This radar facies is interpreted to represent washover deposits, possibly into an older lagoon. The third facies, RF_{sbf} is composed of subhorizontal, nearly flatlying reflections. The individual

reflections are not as continuous as some of the reflections of the other facies. This radar facies usually unconformably overlies RF_{sd} or RF_{ld} facies. The RF_{shf} is interpreted to represent eolian dunes overlying older beach foreshore and washover deposits. Ground-penetrating radar profiles through the RF_{sd} facies towards the end of GPR Line 78 (Supplementary Figure 4) contain minor erosional discontinuities repeating cyclically for nearly 500m (Figure 5). Buynevich et al., 2007 and Zurbuchen et al., 2020 interpreted similar features as erosional surfaces cut by large storms. Given the prevalence of hurricanes and other large storms along the Florida Panhandle, a similar interpretation is taken for these erosional scarps.

4.2.2 Interpreted beach-dune contact

The contact beween RF_{sd} and the overying RF_{shf} is interpreted to mark the beach-dune (BD) contact. The elevation of the beach-dune (BD) contact changes through Beach Ridge sets A, B, and C, which were crossed in GPR lines L77, L78 and L79 (Figure 5). The BD contact crosses both Beach Ridge Sets A and B in GPR line L79 (Figure 5, A-A' profile). Within this GPR line the BD contact drops 4.5 m, from a maximum height of 6.3m down to 1.8m (NAVD88, Supplementary GPR-L79). An alluvial infill overlies the seaward dipping beach deposits of RF_{sd} (Supplementary Figure 5) while seaward the BD contact rises again reaching a maximum elevation of 3.9m. Seaward of this change, the BD contact appears to continuously drop until it reaches the current sea level with a 2 mm per meter of prograding beach (Supplementary Figure 4).

A major feature interrupting the prograding beach deposits is an alluvial infill whose origin is linked to a sediment bypass feature (Nienhuis et al., 2016) observed at the beginning of L77. Sediment bypass features usually form when waves approach a river mouth obliquely, setting up a longshore current that transports more sediment along the coast than is brought ashore. Based on L78 (Supplementary Figure 4), the continuity of the beach deposits is interrupted by flat-lying tangent horizons that we interpret as erosional storm scarps (Figure 5, B-B' profile). L77 is less clear since it is affected by fluvial and wave erosion as observed on both east and west sides of the profile.

Farther north, within Beach Ridge Set C (Figure 5), GPR facies RF_{sd} is also found in GPR line L91 (Supplementary Figure 6). Within this beach ridge set, the BD contact is found at a nearly constant elevation of 5.9m for 1km and gradually decreases seaward to 2.6m over a distance of 0.9km (Supplementary Figure 6). Erosional features interpreted as storm events are also apparent in this unit (Figure 5, C-C' profile), similar to GPR-L78 in Beach Ridge Set A. Tracing L91 from south (C) to north (C'), an extended erosional surface interrupts the beach progradation at line distance ~360m, followed by a zone of hyperbolic reflections, suggesting a different depositional environment (Supplementary Figure 6).

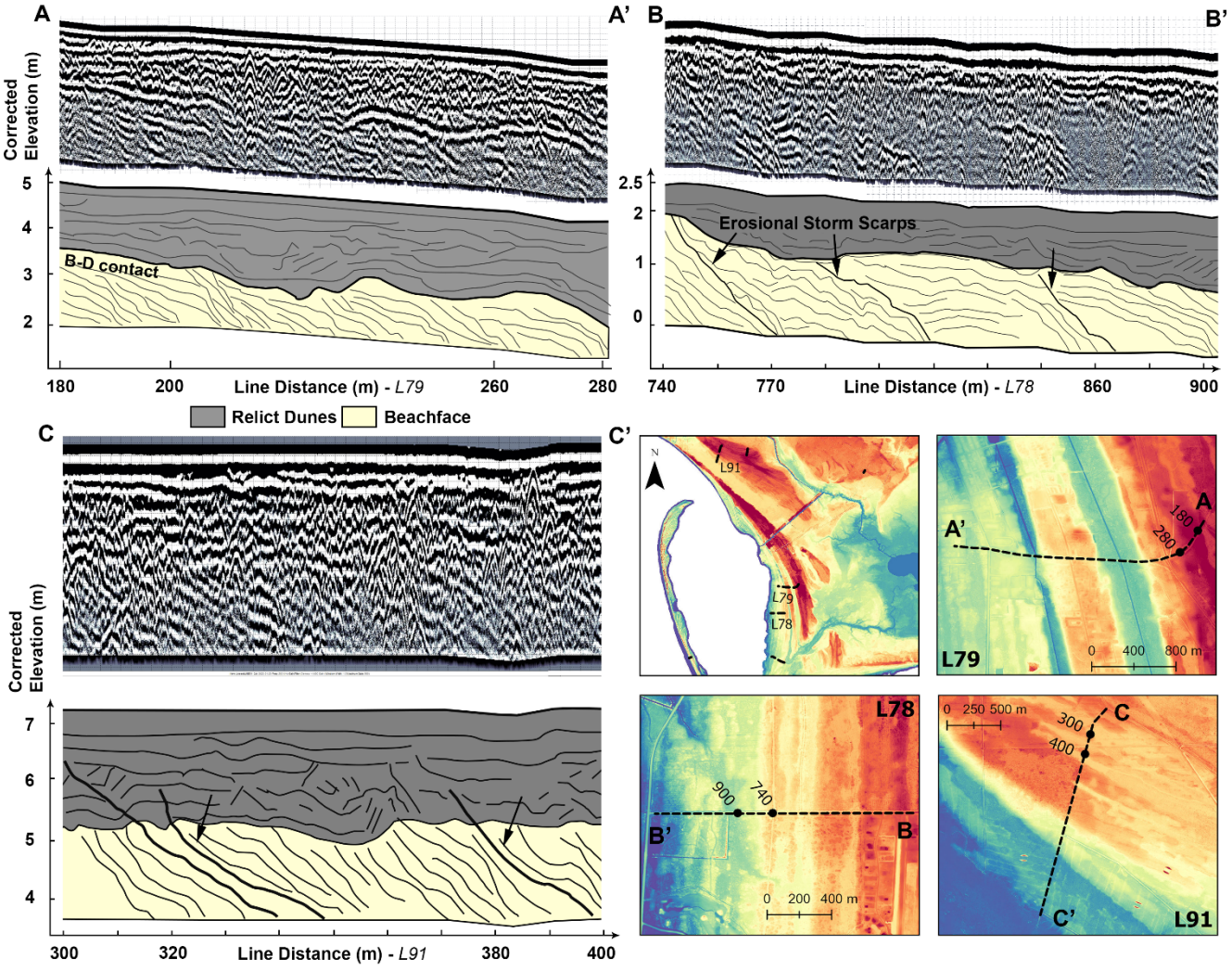

Figure 5. Location of GPR profiles and interpretation for GPR lines L79, L78, and L91 (see full profiles and interpretation of radar surfaces in Supplementary Figures 4,5 and 6). The profile locations are plotted on top of the 1-meter resolution DEMs (US Geological Survey, 2022).

4.3 Interpreted beach ridge set ages

Based on the OSL dates acquired by Burdette et al., 2012 from Beach Ridge Set A (Figure 3Figure 5B), the surficial beach ridges surveyed in GPR lines 77, 78, and the seaward most reaches of 79 have an average age of 114±9 ka BP. Beach Ridge Set B appears to be onlapped by Beach Ridge Set A. A similar architecture as that found in our Beach Ridge Sets A and B is found to the east underlying another transect of OSL-dated cores by Burdette et al. (2012). The equivalent of our Beach Ridge Set B in that profile of cores has an average OSL age of 132±12 ka BP (Figure 3Figure 5B). We interpret these two Beach Ridge Sets A and B as two distinct periods of beach ridge strandplain progradation. The younger Beach Ridge Set A ranges in

elevation from 0 to 4.5m and we propose that it formed in late MIS5e. MIS 6 deposits were dated by Burdette et al., 2012 below marine/coastal sediments associated with a second, more landward ridge (Figure 3Figure 5). We propose that the older Beach Ridge Set B formed during early MIS 5e. Beach Ridges Set C located farther inland and ranges in elevation from 4.3m to 8.5m. It is disconnected from the two seaward Beach Ridge Sets A and B (Figure 3Figure 5). We suggest that this strandplain, surveyed in GPR line L91 (Figure 3Figure 5 and Supplementary Figure 6), is older than the Last Interglacial and may represent the imprint of a former highstand (MIS7, MIS 9 or MIS11). In the following text, we explore this hypothesis, while noting that an early MIS 5e age for Beach Ridge Set C cannot be excluded *a priori* without radiometric ages.

5.0 Discussion

5.1 Pleistocene relative sea-level changes

From the descriptions above, GPR profiles L78, L79 and L91 preserved the clearest and most continuous evidence of the Beach-Dune (BD) contact. Applying the indicative meaning of the modern BD contact (Figure 4Figure 3) to the elevation of the BD contact along these profiles allows the reconstruction of relative sea-level (RSL) changes during the late Pleistocene. Overall, the most striking features are the suggested RSL oscillations identified in the GPR profiles.

GPR Line 91 runs through Beach Ridge Set C interpreted to have formed during an interglacial older than MIS 5e. RSL remains stable for enough time for the beach to prograde 1.0 km before falling to 2.6 m (Figure 6A). For Beach Ridge Sets A and B, higher sea levels are recorded for Beach Ridge Set B in GPR Line 79 (Figure 6B), which we correlate to early MIS 5e, than Beach Ridge Set A, which we corelate to late MIS5e. Starting from a peak RSL of ~5m, like the initial RSL in GPR Line 91, RSL drops then rises rapidly to 4m above present (Figure 6B). Sea level then falls again (Figure 6B). GPR Line 78 indicates continued sea-level fall through the end of the LIG recorded in our profiles (Figure 6C).

5.2 Potential RSL implications

Without a precise age assignments for Beach Ridge Sets A and B, it is prudent to remain cautious in speculating about the origins of the MIS-5e RSL oscillation that we propose. Nevertheless, their relative age based on stratigraphic superposition, enable us to weigh several possible origins. First, the RSL oscillation could be caused by the isostatic response to sediment loading and unloading of the shelf during phases of increased or decreased sedimentation from the Apalachicola River delta. Sediment isostasy is capable of driving departures from eustasy of several meters between the present interglacial and the LIG (Simms et al., 2013; Pico, 2020), in particular in areas with rapid sedimentation such as the northern Gulf of Mexico. However, magnitudes of land motion calculated for the LIG (Simms et al., 2013) and Holocene (Kuchar et al., 2018) shorelines outside of the Mississippi Delta are too low to fully explain the swings suggested by our GPR data.

Next, we consider ice sheet melt and glacial isostatic adjustment as origins for the Apalachicola RSL oscillation. Because the Apalachicola Delta sits on the Laurentide Ice Sheet's peripheral bulge, RSL is sensitive to solid Earth effects associated with Laurentide melt as well as the fingerprints of Antarctic and Greenland excess melt. Antarctic Ice Sheet reconstructions during MIS-5e consistently find excess melt of >3m global mean sea level equivalent prior to 126 ka (Barnett et al., 2023; Golledge et al., 2021; Kopp et al., 2009), a contribution supported by evidence that the West Antarctic Ice Sheet collapsed during MIS-5e (Lau et al., 2023) and prior to 126 ka (Wolff et al., 2025), accompanied by substantial East Antarctic melt (Iizuka et al., 2023).

Early MIS-5e Antarctic collapse was likely accompanied by delayed Northern Hemisphere ice sheet melt. Mounting evidence supports Laurentide remnants persisting into early MIS-5e. For example, North Atlantic red layers dated to ~125-6 ka (Nicholl et al., 2012; Zhou and McManus, 2022) resemble cores of ~8.2 ka age deposited when a proglacial lake burst through the Laurentide and flooded the Labrador Sea (Jennings et al., 2015; Kerwin, 1996). These cores imply an outburst flood at ~125-6 ka similar to the 8.2 ka event flood, which requires a Laurentide of ~3+m GMSL equivalent volume (Zhou and McManus, 2022) and aligns with Labrador Sea isotope data showing glacial erosion of the Canadian craton through 126 ka (Parker and Harrison, 2022). An early MIS-5e Laurentide would have cooled the Northern Hemisphere (Hirose et al., 2025) despite high insolation forcing (Quiquet and Roche, 2024) and would help explain lower-than-present Norwegian Sea sea surface temperatures (SST) from 128 - 126.5 ka (Ezat et al., 2024); freshwater plumes and iceberg rafted debris leaving the Labrador Sea at ~126 ka (Irvalı et al., 2016, 2012); and early MIS-5e SST proxies that lag behind ice volume proxies in the North Atlantic (Cline et al., 1984). Similarly, nearly all MIS-5e Greenland Ice Sheet volume estimates from the last decade place the ice sheet's peak contribution at 1-3 m GMSL equivalent after ~125 ka, in sync with the Northern Hemisphere summer insolation maximum at ~122 ka (Creel and Austermann, 2025).

The melting and regrowing of Earth's ice sheets at different times during MIS-5e could have contributed to an oscillation in Apalachicola RSL both through changes in GMSL and through glacial isostatic adjustment, which describes the viscoelastic response of the solid Earth to changes in ice and water loading (Farrell and Clark, 1976). When out of phase, ice sheet contributions to GMSL can mask each other (Raymo et al., 2006). Thus, whether MIS-5e GMSL oscillated by <1m (Dyer et al., 2021) or <4m (Kopp et al., 2013), much larger fluctuations in individual ice sheets could have occurred so long as the timing of peak melt varied. And because of the differing sea-level fingerprints of each ice sheet (Hay et al., 2014), these ice sheet asymmetries could have led to rapid fluctuations in Apalachicola sea level.

Even without GMSL changes, the glacial isostatic adjustment (GIA) associated with asymmetric MIS-5e ice sheet melt could have led to a multi-meter oscillation in local sea level in the Gulf of Mexico (Creel and Austermann, 2025, Figure 6D). Creel and Austermann (2025) built an ensemble of ice sheet simulations in which simultaneous early MIS-5e Laurentide persistence and West Antarctic collapse balance to yield constant interglacial global mean sea level. We used this ensemble to find that

because of GIA, simultaneous early MIS-5e Laurentide persistence and West Antarctic collapse can cause Apalachicola RSL to rise by 20+ mm/yr (early MIS-5e), then fall by up to -2 mm/yr, then rise by +2 mm/yr, then fall by 3-5+ mm/yr in late MIS-5e (Figure 6D). These magnitudes and tendencies are within the range of our RSL changes inferred from GPR. This suggests that the concurrent but asymmetric melt and regrowth of multiple ice sheets may be needed to explain the rapid RSL changes we observe.

The most probable candidate for rapid melt and regrowth is the West Antarctic Ice Sheet (WAIS), for two reasons. First, each 1 mm/yr of WAIS melt/regrowth would increase/decrease Apalachicola RSL by ~1.3 mm/yr due to the fingerprint of WAIS ice melt (Hay et al., 2014). Second, WAIS collapse in early MIS-5e was likely triggered by ocean forcing (Clark et al., 2020). Once that warm water incursion abated, the low insolation during austral summer would have enabled some sectors of WAIS to regrow rapidly, as is suggested by the presence of the Ronne Ice Shelf by 126 ka (Wolff et al., 2025). The overlapping effects of WAIS regrowth, Laurentide Hudson Bay ice saddle collapse during the MIS-5e proglacial lake flooding event (Zhou and McManus, 2022), and concurrent Greenland melt (Yau et al., 2016), could have summed to magnitudes of RSL change similar to the changes we observed along the Apalachicola coast. This scenario would also better align the Apalachicola RSL rates with MIS-5e sea-level rates reported in the Red Sea (Rohling et al., 2019, Figure 6E), as the Red Sea WAIS fingerprint is ~75% that of Apalachicola (Hay et al., 2014).

5.3 Other Late Pleistocene environmental records

In addition to the RSL pattern, in the latter part of GPR Line 78, we identified seven erosional surfaces in Beach Ridge Set A that we interpreted as erosion from storms (Figure 5, Figure 6C). From our age interpretations, these seven erosional features were created during the very last part of MIS 5e (i.e., around 113-117 ka, Figure 8E). Applying Holocene barrier progradation rates in this area, published by different authors (Forrest, 2007; Rink and López, 2015, 2010) and averaging only the long-term rates (>1 ka) obtained in this area (see Supplementary Table 1), we obtain that the long-term average barrier progradation rate in this area is 1.18 m/yr.

Therefore, assuming a progradation rate equal to that during the Holocene of 1.18 m/, these seven storms happened over a period of ~540 years. This translates to a recurrence of one major storm every 76 years during late MIS 5e. This recurrence interval is lower than the historical record of hurricanes (one every 42 years, Rodysill et al., 2020), but higher than the estimated 12 extreme hurricanes over ~2500 years proposed for the Gulf of Mexico by Bregy et al. (2018). The greater frequency of storms during the historical record may suggest the GPR only captures events above a certain magnitude threshold (e.g., hurricane category ≥3), or that beach ridge formation is influenced primarily by such high-intensity events, whereas sediment cores may preserve a broader range of storm imprints.

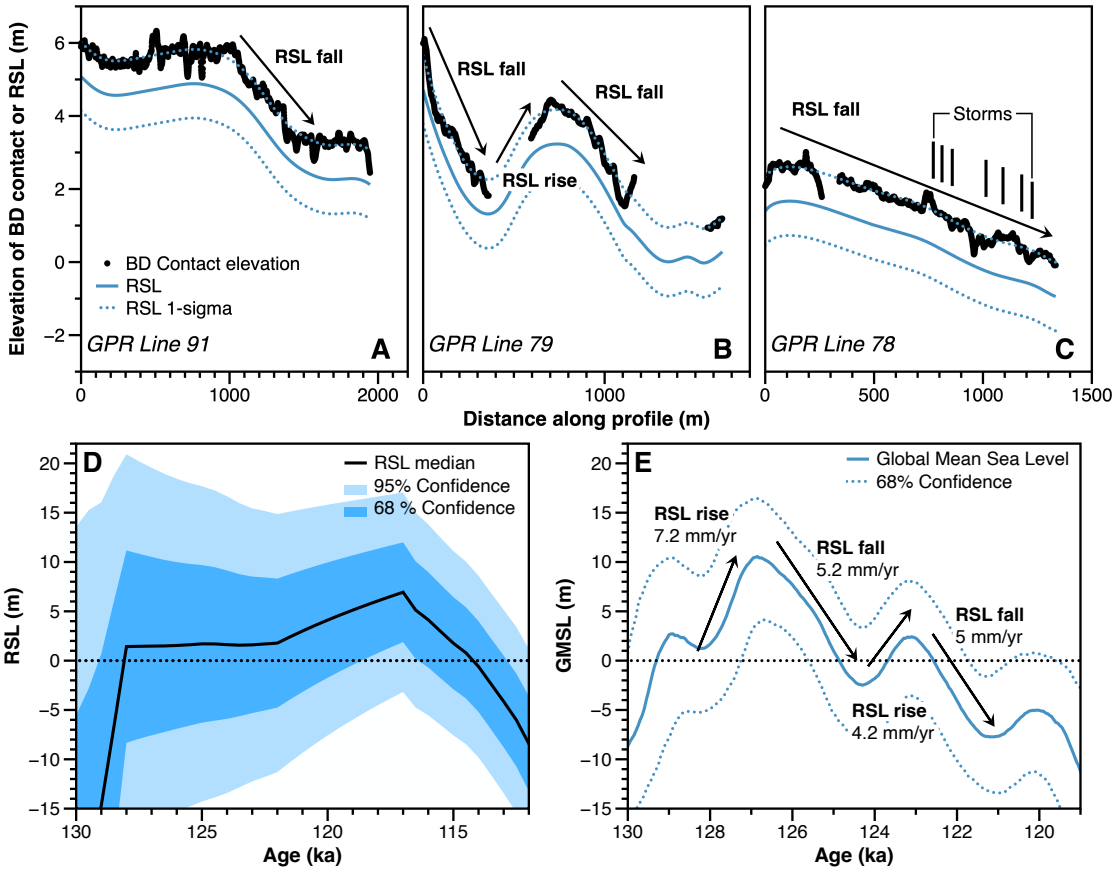

Figure 6. A) Beach-Dune contact and associated RSL at GPR Line 91, interpreted as pre-MIS 5e (see text for discussion). B) and C) Same as A), but for GPR Lines 79 and 78, respectively representative of early / mid and late MIS 5e (see text for discussion). D) GIA relative sea level as predicted by glacial isostatic adjustment models at Cape San Blas (Creel and Austermann, 2025). E) GMSL during MIS 5e and associated rates as calculated by Rohling et al., 2019.

5.4 Paleogeographical evolution of the Apalachicola Barrier Island Complex

Our results suggest that a coastal barrier system prograded during the early MIS5e highstand forming a series of east-west oriented barrier islands and a north-south oriented strandplain attached on its west to older Pleistocene deposits (Figure 7A). During the MIS5e RSL fall (Figure 7B), the delta of the ancestral Apalachicola River prograded, eroding the strandplain and seabed near Cape San Blas and forming the channel now occupied by Depot Creek – which currently flows north but whose tributaries appear to indicate a southward directed flow at one time (Donoghue, 1993). After sea level rose during late MIS5e, the small river in Cape San Blas was bypassed and younger beach ridges nucleated from the Early MIS5e deposits (Figure 7C). Finally, during the Holocene transgression new smaller barrier islands formed south of the Pleistocene coastal barrier system. These islands, located along Cape San Blas, connected to the Pleistocene units as the Apalachicola River now rerouted to enter the Gulf east of its late MIS5e location (Figure 7D).

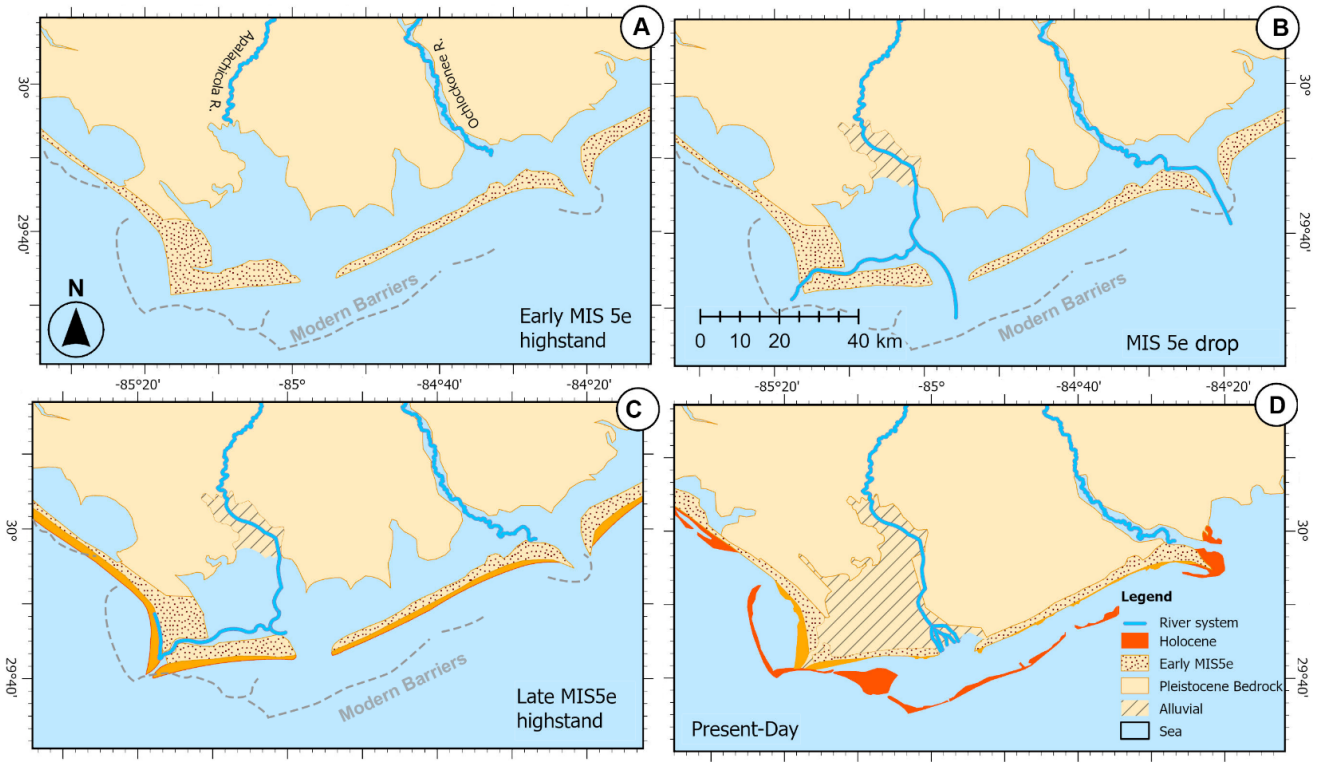

Figure 7. Evolution of the Apalachicola coastal barrier system since the Last Interglacial (MIS5e). A) Early MIS 5e highstand; B). MIS5e drop, C) Late MIS5e highstand, D) Present-day coastal morphology.

6. Conclusions

We acquired new Ground Penetrating Radar (GPR) profiles and RTK measurements across modern and fossil beach ridges and strandplains in the Apalachicola River Delta area of northwest Florida. Combined with existing LiDAR-derived digital elevation models (DEMs) and Optically Stimulated Luminescence (OSL) ages, these data provide new insights into the region's response to sea-level changes over geological timescales. Based on this integrated analysis, we propose a coastal barrier evolution model for the broader Apalachicola Delta area from at least the Last Interglacial (MIS 5e) through the present. Our results suggest marine deposits extended across the Apalachicola Delta from elevations as high as +75 meters (NAVD88) down to mean sea level, likely representing sedimentation from the Late Pliocene to Early Pleistocene. Coastal landforms such as spits, barriers, and sandbars are recognized, attesting to the long and dynamic coastal history of the area.

Within the Pleistocene coastal sequences, GPR, LiDAR, and OSL data reveal the existence of two distinct beach ridge units formed during the early and late phases of MIS 5e. The MIS5e units appear to have been shaped by sea-level oscillations. We propose that the observed oscillations are linked to the regrowth of a collapsed West Antarctic Ice Sheet, coinciding with ongoing Laurentide and Greenland ice melt during MIS 5e. Further inland, we identified a third, stratigraphically older beach

ridge plain, likely formed during a previous interglacial period (MIS 7, or older), although an early MIS 5e age cannot be excluded. The presence of MIS 6 alluvial deposits and better-preserved coastal sequences in the western delta supports the interpretation of a complex, multi-phase Pleistocene evolution.

Additionally, erosional scarps identified in GPR profiles suggest the occurrence of major storm events approximately every 76 years during the latter part of MIS 5e, highlighting the dynamic interplay between storm activity and barrier development; however, this estimate is tentative, as it depends on assumptions about progradation rates, GPR resolution and the preservation of only higher-magnitude events.

Supplementary Information

All data and supplementary figures mentioned in the text are available open-access at this link: https://doi.org/10.5281/zenodo.15202796

A preprint of this manuscript was submitted on May 4th, 2025 to EarthArXiv.

Acknowledgements

This work was funded by the European Research Council (ERC) under the European Union's Horizon 2020 research and innovation programme (grant agreement n. 802414). The manuscript reflects only the view of the authors and the EU is not responsible for any use that may be made of the information it contains. RC was supported by a Woods Hole Oceanographic Institution Postdoctoral Scholarship'.

References

Barnett, R.L., Austermann, J., Dyer, B., Telfer, M.W., Barlow, N.L., Boulton, S.J., Carr, A.S., Creel, R.C., 2023. Constraining the contribution of the Antarctic Ice Sheet to Last Interglacial sea level. Sci. Adv. 9, eadf0198.

Boyd, R., Dalrymple, R., Zaitlin, B., 1992. Classification of clastic coastal depositional environments. Sediment. Geol. 80, 139–150.

Bregy, J.C., Wallace, D.J., Totten, R.L., Cruz, V.J., 2018. 2500-year paleotempestological record of intense storms for the northern Gulf of Mexico, United States. Mar. Geol. 396, 26–42. https://doi.org/10.1016/j.margeo.2017.09.009

Brenneman, L., Tanner, W.F., 1958. Possible abandoned barrier islands in panhandle Florida. J. Sediment. Res. 28, 342–344.

Burdette, K.E., Rink, W.J., López, G.I., Mallinson, D.J., Parham, P.R., Reinhardt, E.G., 2012. Geological investigation and optical dating of Quaternary siliciclastic sediments near Apalachicola, North-west Florida, USA. Sedimentology 59, 1836–1849. https://doi.org/10.1111/j.1365-3091.2012.01328.x

Buynevich, I.V., FitzGerald, D.M., Goble, R.J., 2007. A 1500 yr record of North Atlantic storm activity based on optically dated relict beach scarps. Geology 35, 543–546.

Carruthers, E.A., Lane, D.P., Evans, R.L., Donnelly, J.P., Ashton, A.D., 2013. Quantifying overwash flux in barrier systems: An example from Martha's Vineyard, Massachusetts, USA. Mar. Geol. 343, 15–28.

Carvalho, R.C., Oliver, T.S.N., Woodroffe, C.D., 2019. Transition from marine to fluvial-dominated sediment supply at Shoalhaven prograded barrier, southeastern Australia. Geomorphology 341, 65–78. https://doi.org/10.1016/j.geomorph.2019.05.010

Clark, P.U., He, F., Golledge, N.R., Mitrovica, J.X., Dutton, A., Hoffman, J.S., Dendy, S., 2020. Oceanic forcing of penultimate deglacial and last interglacial sea-level rise. Nature 577, 660–664.

Cline, R.M.L., Hays, J.D., Prell, W.L., Ruddiman, W.F., Moore, T.C., Kipp, N.G., Molfino, B.E., Denton, G.H., Hughes, T.J., Balsam, W.L., Brunner, C.A., Duplessy, J.-C., Esmay, A.G., Fastook, J.L., Imbrie, J., Keigwin, L.D., Kellogg, T.B., McIntyre, A., Matthews, R.K., Mix, A.C., Morley, J.J., Shackleton, N.J., Streeter, S.S., Thompson, P.R., 1984. The Last Interglacial Ocean. Quat. Res. 21, 123–224. https://doi.org/10.1016/0033-5894(84)90098-X

Costas, S., Ferreira, Ó., Plomaritis, T.A., Leorri, E., 2016. Coastal barrier stratigraphy for Holocene high-resolution sea-level reconstruction. Sci. Rep. 6, 38726. https://doi.org/10.1038/srep38726

Creel, R.C., Austermann, J., 2025. Glacial isostatic adjustment driven by asymmetric ice sheet melt during the Last Interglacial causes multiple local sea-level peaks. Geology 53, 253–258. https://doi.org/10.1130/G52483.1

Donnelly, C., Kraus, N., Larson, M., 2006. State of knowledge on measurement and modeling of coastal overwash. J. Coast. Res. 22, 965–991.

Donoghue, J.F., 1993. Late Wisconsinan and Holocene depositional history, northeastern Gulf of Mexico. Mar. Geol. 112, 185–205.

Donoghue, J.F., Stapor, F.W., Tanner, W.F., 1998. Discussion of: Otvos, EG, 1995. Multiple Pliocene-Quaternary Marine Highstands, Northeast Gulf Coastal Plain-Fallacies and Facts. Journal of Coastal Research, 11, 984-1002. J. Coast. Res. 669–674.

Dougherty, A.J., 2018. Prograded coastal barriers provide paleoenvironmental records of storms and sea level during late Quaternary highstands. J. Quat. Sci. 33, 501–517.

Dyer, B., Austermann, J., D'Andrea, W.J., Creel, R.C., Sandstrom, M.R., Cashman, M., Rovere, A., Raymo, M.E., 2021. Sea-level trends across the Bahamas constrain peak last interglacial ice melt. Proc. Natl. Acad. Sci. U. S. A. 118, 1–11. https://doi.org/10.1073/pnas.2026839118

Ezat, M.M., Fahl, K., Rasmussen, T.L., 2024. Arctic freshwater outflow suppressed Nordic Seas overturning and oceanic heat transport during the Last Interglacial. Nat. Commun. 15, 8998. https://doi.org/10.1038/s41467-024-53401-3

Fairbridge, R.W., Hillaire-Marcel, C., 1977. An 8,000-yr palaeoclimatic record of the 'Double-Hale'45-yr solar cycle. Nature 268, 413–416.

Farrell, W., Clark, J.A., 1976. On postglacial sea level. Geophys. J. Int. 46, 647–667.

Flemming, B., 1982. Xi. Beach morphodynamics in relationship to wave energy, grain size and internal sedimentary structure. Jt. Geol. Surv. Cape Town 97.

Forrest, B.M., 2007. Evolution of the beach ridge strandplain on st. Vincent island, florida (Ph.D. Thesis). The Florida State University.

Gernant, C., Simms, A.R., DeWitt, R., Theilen, B., Garcia, C.N., Goebel, M., 2025. Insights into the sea-level history of the South Shetland Islands from ground penetrating radar on Livingston Island, Antarctica. Quat. Sci. Rev. 359, 109363.

Goetschius, D.W., 1971. Preliminary sedimentological and geomorphological study of certain high terrace sands between the Ochlockonee and Apalachicola rivers, Liberty and Gadsden Counties, Florida (PhD Thesis). Florida State University.

Golledge, N.R., Clark, P.U., He, F., Dutton, A., Turney, C.S.M., Fogwill, C.J., Naish, T.R., Levy, R.H., McKay, R.M., Lowry, D.P., Bertler, N.A.N., Dunbar, G.B., Carlson, A.E., 2021. Retreat of the Antarctic Ice Sheet During the Last Interglaciation and Implications for Future Change. Geophys. Res. Lett. 48, e2021GL094513. https://doi.org/10.1029/2021GL094513

Goodwin, I.D., Mortlock, T.R., Ribo, M., Mitrovica, J.X., O'Leary, M., Williams, R., 2023. Robbins Island: The index site for regional Last Interglacial sea level, wave climate and the subtropical ridge around Bass Strait, Australia. Quat. Sci. Rev. 305, 107996.

Goslin, J., Clemmensen, L.B., 2017. Proxy records of Holocene storm events in coastal barrier systems: Storm-wave induced markers. Quat. Sci. Rev. 174, 80–119. https://doi.org/10.1016/j.quascirev.2017.08.026

Hay, C., Mitrovica, J.X., Gomez, N., Creveling, J.R., Austermann, J., Kopp, R.E., 2014. The sea-level fingerprints of ice-sheet collapse during interglacial periods. Quat. Sci. Rev. 87, 60–69.

Hede, M.U., Bendixen, M., Clemmensen, L.B., Kroon, A., Nielsen, L., 2013. Joint interpretation of beach-ridge architecture and coastal topography show the validity of sea-level markers observed in ground-penetrating radar data. The Holocene 23, 1238–1246.

Hein, C.J., Ashton, A.D., 2020. Long-term shoreline morphodynamics: processes and preservation of environmental signals. Sandy Beach Morphodynamics 487–531.

Hesp, P.A., 1984. Foredune formation in southeast Australia, in: Coastal Geomorphology in Australia. Academic Press, pp. 69–97.

Hirose, L.A., Abe-Ouchi, A., Chan, W.-L., O'ishi, R., Yoshimori, M., Obase, T., 2025. Arctic Warming Suppressed by Remnant Glacial Ice Sheets in Past Interglacials. Geophys. Res. Lett. 52, e2024GL111798. https://doi.org/10.1029/2024GL111798

Holdahl, S.R., Morrison, N.L., 1974. Regional investigations of vertical crustal movements in the US, using precise relevelings and mareograph data. Tectonophysics 23, 373–390.

Iizuka, M., Seki, O., Wilson, D.J., Suganuma, Y., Horikawa, K., van de Flierdt, T., Ikehara, M., Itaki, T., Irino, T., Yamamoto, M., Hirabayashi, M., Matsuzaki, H., Sugisaki, S., 2023. Multiple episodes of ice loss from the Wilkes Subglacial Basin during the Last Interglacial. Nat. Commun. 14, 2129. https://doi.org/10.1038/s41467-023-37325-y

Irvalı, N., Ninnemann, U.S., Galaasen, E.V., Rosenthal, Y., Kroon, D., Oppo, D.W., Kleiven, H.F., Darling, K.F., Kissel, C., 2012. Rapid switches in subpolar North Atlantic hydrography and climate during the Last Interglacial (MIS 5e). Paleoceanography 27. https://doi.org/10.1029/2011PA002244

Irvalı, N., Ninnemann, U.S., Kleiven, H. (Kikki) F., Galaasen, E.V., Morley, A., Rosenthal, Y., 2016. Evidence for regional cooling, frontal advances, and East Greenland Ice Sheet changes during the demise of the last interglacial. Quat. Sci. Rev. 150, 184–199. https://doi.org/10.1016/j.quascirev.2016.08.029

Isla, M.F., Moyano-Paz, D., FitzGerald, D.M., Simontacchi, L., Veiga, G.D., 2023. Contrasting beach-ridge systems in different types of coastal settings. Earth Surf. Process. Landf. 48, 47–71.

Jennings, A., Andrews, J., Pearce, C., Wilson, L., Ólfasdóttir, S., 2015. Detrital carbonate peaks on the Labrador shelf, a 13–7ka template for freshwater forcing from the Hudson Strait outlet of the Laurentide Ice Sheet into the subpolar gyre. Quat. Sci. Rev. 107, 62–80. https://doi.org/10.1016/j.quascirev.2014.10.022

Jol, H.M., Smith, D.G., Meyers, R.A., 1996. Digital ground penetrating radar (GPR): a new geophysical tool for coastal barrier research (examples from the Atlantic, Gulf and Pacific Coasts, USA). J. Coast. Res. 960–968.

Kerwin, M.W., 1996. A Regional Stratigraphic Isochron (ca. 800014C yr B.P.) from Final Deglaciation of Hudson Strait. Quat. Res. 46, 89–98. https://doi.org/10.1006/qres.1996.0049

Komar, P.D., Wang, C., 1984. Processes of selective grain transport and the formation of placers on beaches. J. Geol. 92, 637–655.

Kopp, R.E., Simons, F.J., Mitrovica, J.X., Maloof, A.C., Oppenheimer, M., 2013. A probabilistic assessment of sea level variations within the last interglacial stage. Geophys. J. Int. 193, 711–716. https://doi.org/10.1093/gji/ggt029

Kopp, R.E., Simons, F.J., Mitrovica, J.X., Maloof, A.C., Oppenheimer, M., 2009. Probabilistic assessment of sea level during the last interglacial stage. Nature 462, 863–867. https://doi.org/10.1038/nature08686

Kuchar, J., Milne, G., Wolstencroft, M., Love, R., Tarasov, L., Hijma, M., 2018. The Influence of Sediment Isostatic Adjustment on Sea Level Change and Land Motion Along the U.S. Gulf Coast. J. Geophys. Res. Solid Earth 123, 780–796. https://doi.org/10.1002/2017JB014695

Kumar, R., Switzer, A.D., Gouramanis, C., Bristow, C.S., Shaw, T.A., Jankaew, K., Li, T., Brill, D., 2024. Late-Holocene sea-level markers preserved in a beach ridge system on Phra Thong Island, Thailand. Geomorphology 465, 109405.

Lau, S.C.Y., Wilson, N.G., Golledge, N.R., Naish, T.R., Watts, P.C., Silva, C.N.S., Cooke, I.R., Allcock, A.L., Mark, F.C., Linse, K., Strugnell, J.M., 2023. Genomic evidence for West Antarctic Ice Sheet collapse during the Last Interglacial. Science 382, 1384–1389. https://doi.org/10.1126/science.ade0664

Masselink, G., Kroon, A., Davidson-Arnott, R.G.D., 2006. Morphodynamics of intertidal bars in wave-dominated coastal settings — A review. Geomorphology 73, 33–49. https://doi.org/10.1016/j.geomorph.2005.06.007

Masselink, G., van Heteren, S., 2014. Response of wave-dominated and mixed-energy barriers to storms. Mar. Geol. 352, 321–347.

Mauz, B., Hijma, M., Amorosi, A., Porat, N., Galili, E., Bloemendal, J., 2013. Aeolian beach ridges and their significance for climate and sea level: Concept and insight from the Levant coast (East Mediterranean). Earth-Sci. Rev. 121, 31–54.

Maxwell, R., 1971a. Preliminary ionium date from marine terrace, Florida. Coast. Res. Notes 3, 9–10.
Maxwell, R., 1971b. Origin and chronology of Alabama River terraces. GCAGS Trans.
Montes, A., Bujalesky, G.G., Paredes, J.M., 2018. Geomorphology and internal architecture of Holocene sandy-gravel beach ridge plain and barrier spits at Río Chico area, Tierra del Fuego, Argentina. J. South Am. Earth Sci. 84, 172–183.
Nicholl, J.A.L., Hodell, D.A., Naafs, B.D.A., Hillaire-Marcel, C., Channell, J.E.T., Romero, O.E., 2012. A Laurentide outburst flooding event during the last interglacial period. Nat. Geosci. 5, 901–904. https://doi.org/10.1038/ngeo1622
Nielsen, L., Bendixen, M., Kroon, A., Hede, M.U., Clemmensen, L.B., Weβling, R., Elberling, B., 2017. Sea-level proxies in Holocene raised beach ridge deposits (Greenland) revealed by ground-penetrating radar. Sci. Rep. 7, 46460.
Nienhuis, J.H., Ashton, A.D., Giosan, L., 2016. Littoral steering of deltaic channels. Earth Planet. Sci. Lett. 453, 204–214. https://doi.org/10.1016/j.epsl.2016.08.018
NOAA National Centers for Environmental Information, 2023. Coastal Relief Models. NOAA National Centers for Environmental Information. https://doi.org/10.25921/5ZN5-KN44
Nooren, K., Hoek, W.Z., Winkels, T., Huizinga, A., Van Der Plicht, H., Van Dam, R.L., Van Heteren, S., Van Bergen, M.J., Prins, M.A., Reimann, T., Wallinga, J., Cohen, K.M., Minderhoud, P., Middelkoop, H., 2017. The Usumacinta–Grijalva beach-ridge plain in southern Mexico: a high-resolution archive of river discharge and precipitation. Earth Surf. Dyn. 5, 529–556. https://doi.org/10.5194/esurf-5-529-2017
Okazaki, H., Nara, M., Nakazato, H., Furusawa, A., Ito, K., Tamura, T., 2022. Coastal progradation associated with sea-level oscillations in the later phase of the Last Interglacial period, central Japan. Quat. Sci. Rev. 285, 107507.
Olariu, C., Bhattacharya, J.P., 2006. Terminal distributary channels and delta front architecture of river-dominated delta systems. J. Sediment. Res. 76, 212–233.
Otvos, E.G., 2000. Beach ridges — definitions and significance. Geomorphology 32, 83–108. https://doi.org/10.1016/S0169-555X(99)00075-6
Otvos, E.G., 1995. Multiple pliocene-quaternary marine highstands, northeast Gulf Coastal plain: fallacies and facts. J. Coast. Res. 984–1002.
Otvos, E.G., 1992. Quaternary evolution of the Apalachicola coast, northeastern Gulf of Mexico.
Parker, S.E., Harrison, S.P., 2022. The timing, duration and magnitude of the 8.2 ka event in global speleothem records. Sci. Rep. 12, 10542. https://doi.org/10.1038/s41598-022-14684-y
Phillips, M., Blenkinsopp, C., Splinter, K., Harley, M., Turner, I., 2019. Modes of berm and beachface recovery following storm reset: Observations using a continuously scanning lidar. J. Geophys. Res. Earth Surf. 124, 720–736.
Pico, T., 2020. Towards assessing the influence of sediment loading on Last Interglacial sea level. Geophys. J. Int. 220, 384–392. https://doi.org/10.1093/gji/ggz447
Quiquet, A., Roche, D.M., 2024. Investigating similarities and differences of the penultimate and last glacial terminations with a coupled ice sheet–climate model. Clim. Past 20, 1365–1385. https://doi.org/10.5194/cp-20-1365-2024
Raymo, M.E., Lisiecki, L.E., Nisancioglu, K.H., 2006. Plio-Pleistocene Ice Volume, Antarctic Climate, and the Global δ18O Record. Science 313, 492–495. https://doi.org/10.1126/science.1123296
Rink, W.J., López, G.I., 2015. Corrigendum to "OSL-based lateral progradation and aeolian sediment accumulation rates for the Apalachicola Barrier Island Complex, North Gulf of Mexico, Florida" [Geomorphology 123 (2010) 330–342]. Geomorphology 241, 41. https://doi.org/10.1016/j.geomorph.2015.02.016
Rink, W.J., López, G.I., 2010. OSL-based lateral progradation and aeolian sediment accumulation rates for the Apalachicola Barrier Island Complex, North Gulf of Mexico, Florida. Geomorphology 123, 330–342. https://doi.org/10.1016/j.geomorph.2010.08.001
Rodriguez, A.B., Meyer, C.T., 2006. Sea-level variation during the Holocene deduced from the morphologic and stratigraphic evolution of Morgan Peninsula, Alabama, USA. J. Sediment. Res. 76, 257–269.
Rodysill, J.R., Donnelly, J.P., Sullivan, R., Lane, P.D., Toomey, M., Woodruff, J.D., Hawkes, A.D., MacDonald, D., d'Entremont, N., McKeon, K., Wallace, E., Van Hengstum, P.J., 2020. Historically unprecedented Northern Gulf of Mexico hurricane activity from 650 to 1250 CE. Sci. Rep. 10, 19092. https://doi.org/10.1038/s41598-020-75874-0
Rohling, E.J., Hibbert, F.D., Grant, K.M., Galaasen, E.V., Irvalı, N., Kleiven, H.F., Marino, G., Ninnemann, U., Roberts, A.P., Rosenthal, Y., Schulz, H., Williams, F.H., Yu, J., 2019. Asynchronous Antarctic and Greenland ice-volume contributions to the last interglacial sea-level highstand. Nat. Commun. 10, 5040. https://doi.org/10.1038/s41467-019-12874-3

Ruz, M.-H., Allard, M., 1994. Coastal dune development in cold-climate environments. Phys. Geogr. 15, 372–380.
Scheffers, A., Engel, M., Scheffers, S., Squire, P., Kelletat, D., 2012. Beach ridge systems–archives for Holocene coastal events? Prog. Phys. Geogr. 36, 5–37.
Schnable, J.E., Goodell, H.G., 1968. Pleistocene-Recent stratigraphy, evolution, and development of the Apalachicola coast, Florida. Geological Society of America.
Scott, T.M., Campbell, K.M., Rupert, F.R., Arthur, J.D., Missimer, T.M., Lloyd, J.M., Yon, J.W., Duncan, J.G., 2001. Geologic map of the state of Florida. Florida Geological Survey Tallahassee, Fla.
Shennan, I., 1986. Flandrian sea-level changes in the Fenland. II: Tendencies of sea-level movement, altitudinal changes, and local and regional factors. J. Quat. Sci. 1, 155–179. https://doi.org/10.1002/jqs.3390010205
Shennan, I., Long, A.J., Horton, B.P., 2015. Handbook of sea-level research. John Wiley & Sons.
Simms, A.R., John B. Anderson, DeWitt, R., Lambeck, K., Purcell, A., 2013. Quantifying rates of coastal subsidence since the last interglacial and the role of sediment loading. Glob. Planet. Change 111, 296–308. https://doi.org/10.1016/j.gloplacha.2013.10.002
Stapor Jr, F.W., Mathews, T.D., Lindfors-Kearns, F.E., 1991. Barrier-island progradation and Holocene sea-level history in southwest Florida. J. Coast. Res. 815–838.
Stattegger, K., Tjallingii, R., Saito, Y., Michelli, M., Thanh, N.T., Wetzel, A., 2013. Mid to late Holocene sea-level reconstruction of Southeast Vietnam using beachrock and beach-ridge deposits. Glob. Planet. Change 110, 214–222.
Tamura, T., 2012. Beach ridges and prograded beach deposits as palaeoenvironment records. Earth-Sci. Rev. 114, 279–297. https://doi.org/10.1016/j.earscirev.2012.06.004
Tamura, T., Nanayama, F., Saito, Y., Murakami, F., Nakashima, R., Watanabe, K., 2007. Intra-shoreface erosion in response to rapid sea-level fall: depositional record of a tectonically uplifted strand plain, Pacific coast of Japan. Sedimentology 54, 1149–1162.
Taylor, M., Stone, G.W., 1996. Beach-Ridges: A Review. J. Coast. Res. 12.
US Geological Survey, 2022. 1-meter Digital Elevation Model.
US Geological Survey, 2011. National Elevation Dataset, 1/9 arc-second.
Wolff, E.W., Mulvaney, R., Grieman, M.M., Hoffmann, H.M., Humby, J., Nehrbass-Ahles, C., Rhodes, R.H., Rowell, I.F., Sime, L.C., Fischer, H., Stocker, T.F., Landais, A., Parrenin, F., Steig, E.J., Dütsch, M., Golledge, N.R., 2025. The Ronne Ice Shelf survived the last interglacial. Nature 638, 133–137. https://doi.org/10.1038/s41586-024-08394-w
Yau, A.M., Bender, M.L., Robinson, A., Brook, E.J., 2016. Reconstructing the last interglacial at Summit, Greenland: Insights from GISP2. Proc. Natl. Acad. Sci. 113, 9710–9715. https://doi.org/10.1073/pnas.1524766113
Zhou, Y., McManus, J., 2022. Extensive evidence for a last interglacial Laurentide outburst (LILO) event. Geology 50, 934–938. https://doi.org/10.1130/G49956.1
Zurbuchen, J., Simms, A.R., Warrick, J.A., Miller, I.M., Ritchie, A., 2020. A model for the growth and development of wave-dominated deltas fed by small mountainous rivers: Insights from the Elwha River delta, Washington. Sedimentology 67, 2310–2331.

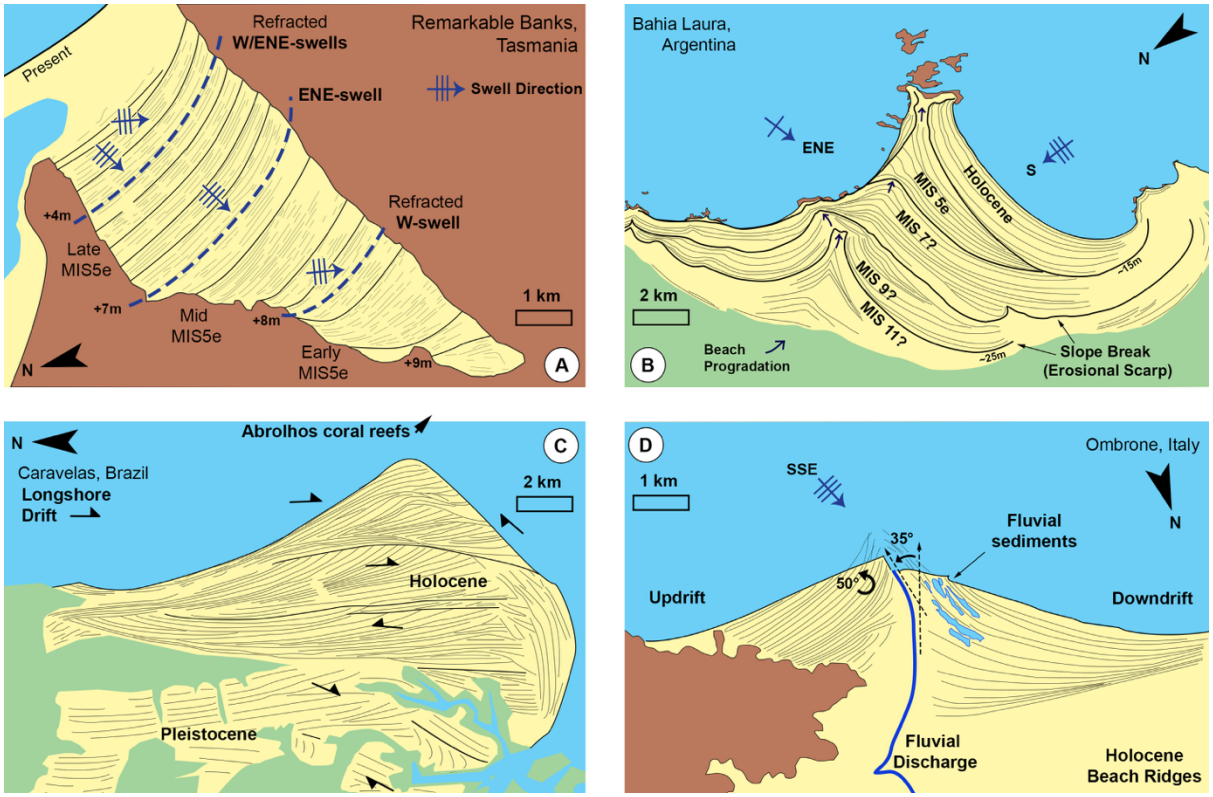

Supplementary Figure 1. Schematic interpretation of beach ridge strandplains on the horizontal plane showing the effect of different processes on the strandplains' geometry: A) Wave-regime shifting (modified after Goodwin et al., 2023). B) uplift and coastal geomorphology (modified after Pedoja et al., 2011- black arrows indicate the influence of rocky outcrops to the evolution of the strandplain). C) longshore drift shift and costal geomorphology (modified after Andrade et al., 2003). D) sediment flux and anthropogenic influence (modified after Mammì et al., 2019; Nienhuis et al., 2016; Pranzini, 2024).

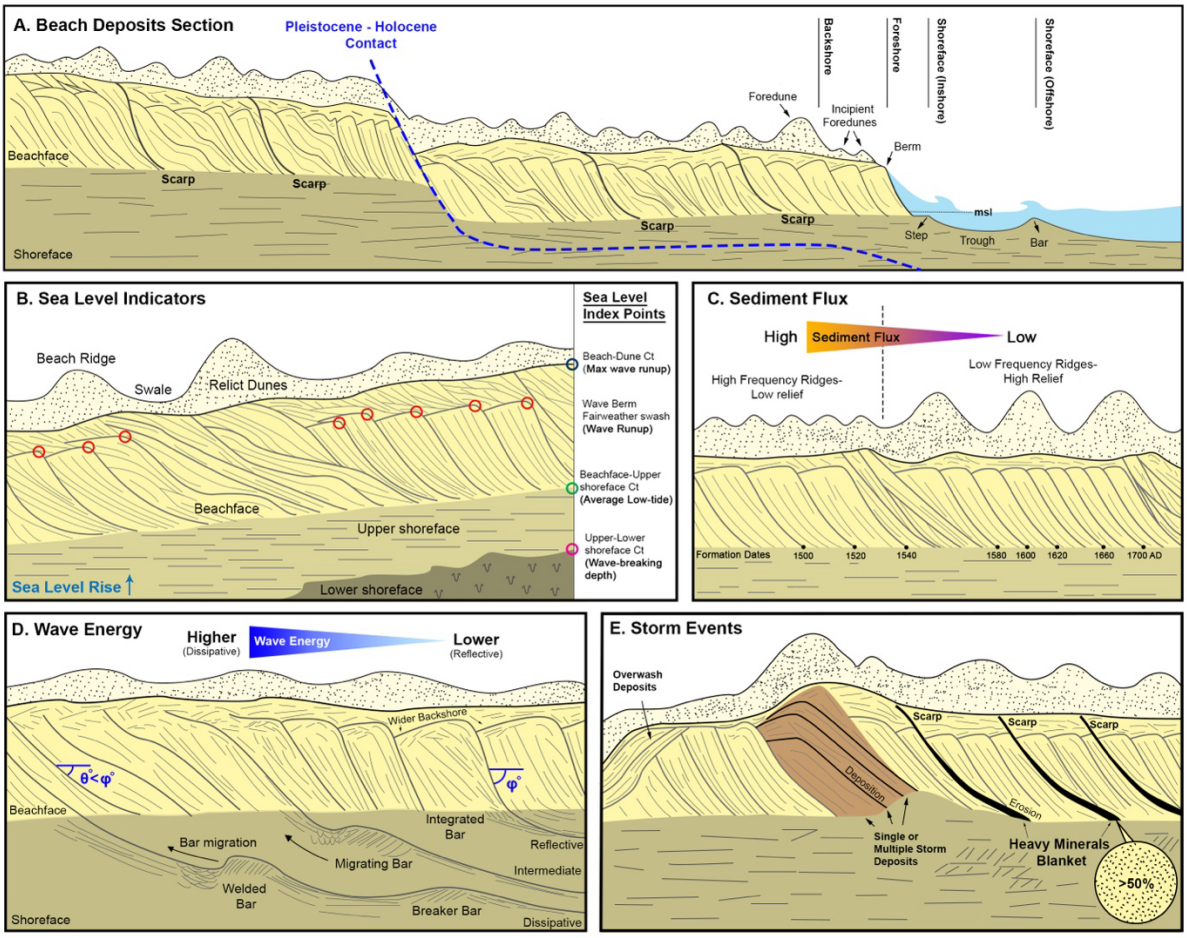

Supplementary Figure 2. Idealized stratigraphic profiles showing common vertical plane geometries and the impact of varying climatic forcings on foreshore and shoreface deposits. A) Composite Holocene-Pleistocene beach deposit section, after Dougherty, 2018. MSL is mean sea level. B) Sea level rise, after Costas et al., 2016. Ct is contact. C) Sediment flux. D) Wave energy. E) Storm events.

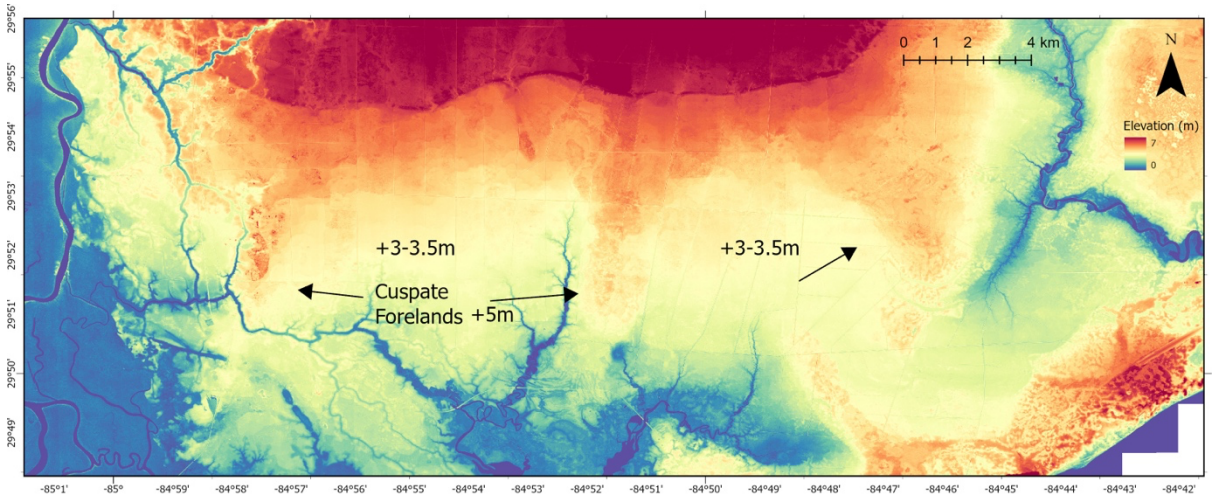

Supplementary Figure 3. Cuspate forelands south of seaward concave features resembling delta fronts (Olariu and Bhattacharya, 2006) on the east side of the Apalachicola River with high-relief seaward crests at elevations of 9.5-10m and 7-7.5m and wide flat areas at 7.5-8m and 6m respectively (NAVD88), seaward of the crests.

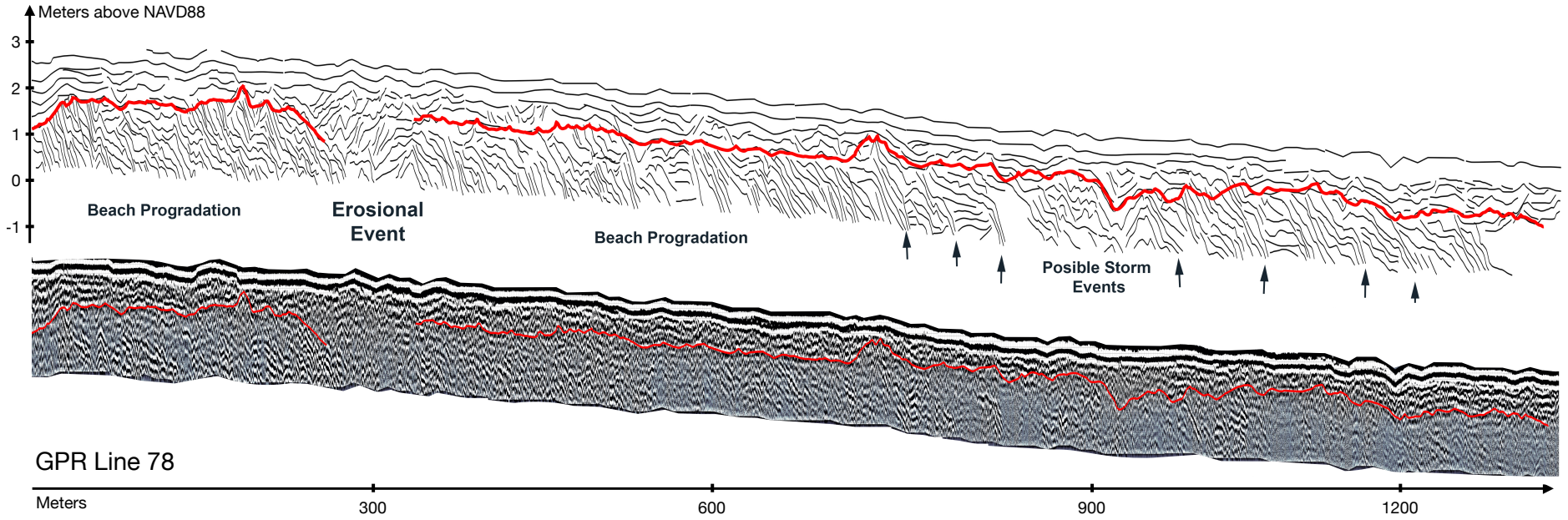

Supplementary Figure 4. GPR Line 78, original radar profile and interpretation

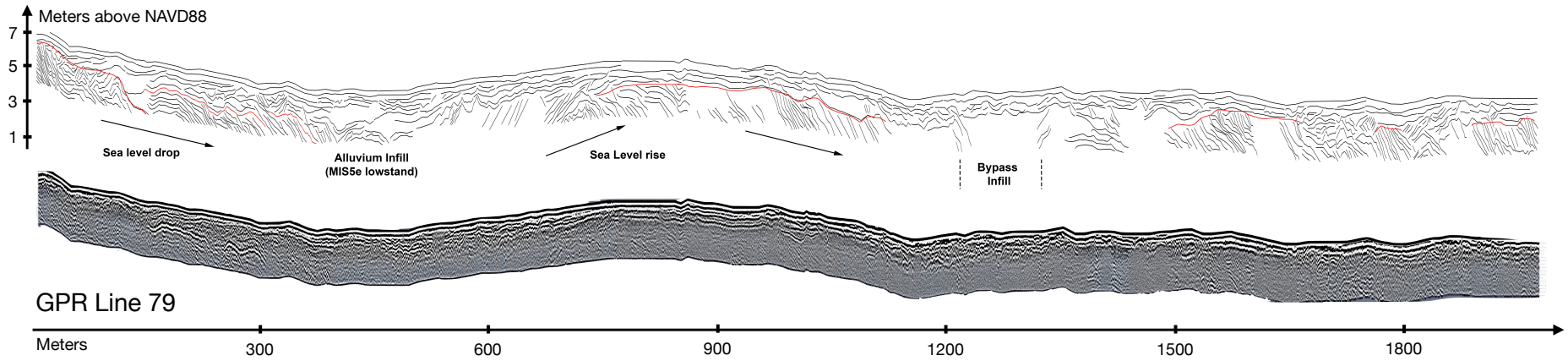

Supplementary Figure 5. GPR Line 79, original radar profile and interpretation

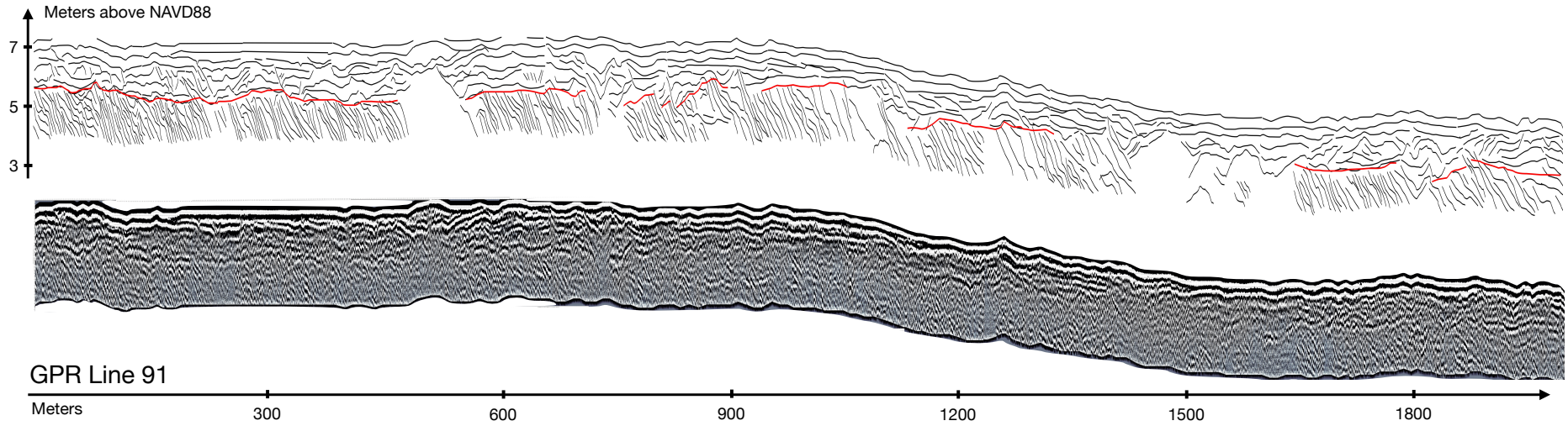

Supplementary Figure 6. GPR Line 91, original radar profile and interpretation

Supplementary Table 1. Progradation rates from cores and associated OSL ages in the Holocene Apalachicola barrier island complex. For full information on the ages, see the source references . Progradation rates were obtained by dividing the distance between two cores and the average ages; errors were propagated considering age uncertainties. * indicates the records used for the average reported in the table's last row. † indicates the lowest progradation rate in the study area.

Location	Source	Age max (yrs)	Age min (yrs)	Distance (m)	Progradation rate (m/yr)
St Vincent Island*	Rink and López, 2010	1890±290	410±60	1300	0.88±0.18
Little St. George Island*	Rink and López, 2010	1900±200	500±50	3050	2.18±0.32
Little St. George Island	Rink and López, 2010	500±50	32±3	1200	2.56±0.27
Little St. George Island*	Rink and López, 2010	1900±200	32±3	4250	2.28±0.24
Cape San Blas	Rink and López, 2015	630±40	330±20	790	2.63±0.39
Cape San Blas	Rink and López, 2015	330±20	0	1400	4.24±0.26
Cape San Blas	Rink and López, 2015	630±40	0	2190	3.48±0.22
St. Joseph Peninsula	Rink and López, 2010	250±20	0	615	2.46±0.20
St. Joseph Peninsula	Rink and López, 2010	600±50	250±20	2419	6.91±1.06
Richardson Hammock	Rink and López, 2010	3300±300	3100±300	450	2.25
St Vincent Island	Forrest, 2007	4100±300	3500±300	2555	4.26±3.01
St Vincent Island*†	Forrest, 2007	3500±300	2500±200	682	0.68±0.25
St Vincent Island*	Forrest, 2007	2500±300	1200±100	1350	1.04±0.25
St Vincent Island	Forrest, 2007	1200±100	800±100	852	2.13±0.75
St Vincent Island	Forrest, 2007	800±100	400	816	2.04±0.51
St Vincent Island	Forrest, 2007	400	0	775	1.94
Weighted mean rates (and associated error) for periods longer than 1000 years					**1.18±0.11**

References

Andrade, A.C.S., Dominguez, J.M.L., Martin, L., Bittencourt, A.C.S.P., 2003. Quaternary evolution of the Caravelas strandplain - Southern Bahia State - Brazil. An. Acad. Bras. Ciênc. 75, 357–382. https://doi.org/10.1590/S0001-37652003000300008

Costas, S., Ferreira, Ó., Plomaritis, T.A., Leorri, E., 2016. Coastal barrier stratigraphy for Holocene high-resolution sea-level reconstruction. Sci. Rep. 6, 38726. https://doi.org/10.1038/srep38726

Dougherty, A.J., 2018. Prograded coastal barriers provide paleoenvironmental records of storms and sea level during late Quaternary highstands. J. Quat. Sci. 33, 501–517.

Goodwin, I.D., Mortlock, T.R., Ribo, M., Mitrovica, J.X., O'Leary, M., Williams, R., 2023. Robbins Island: The index site for regional Last Interglacial sea level, wave climate and the subtropical ridge around Bass Strait, Australia. Quat. Sci. Rev. 305, 107996.

Mammì, I., Rossi, L., Pranzini, E., 2019. Mathematical reconstruction of eroded beach ridges at the Ombrone River Delta. Water 11, 2281.

Nienhuis, J.H., Ashton, A.D., Giosan, L., 2016. Littoral steering of deltaic channels. Earth Planet. Sci. Lett. 453, 204–214. https://doi.org/10.1016/j.epsl.2016.08.018

Olariu, C., Bhattacharya, J.P., 2006. Terminal distributary channels and delta front architecture of river-dominated delta systems. J. Sediment. Res. 76, 212–233.

Pedoja, K., Regard, V., Husson, L., Martinod, J., Guillaume, B., Fucks, E., Iglesias, M., Weill, P., 2011. Uplift of quaternary shorelines in eastern Patagonia: Darwin revisited. Geomorphology 127, 121–142. https://doi.org/10.1016/j.geomorph.2010.08.003

Pranzini, E., 2024. Airborne LIDAR survey applied to the analysis of the historical evolution of the Arno River delta (Italy). J. Coast. Res. 50, 400–409.